Global Urban Road Network Patterns: Unveiling multiscale planning paradigms of 144 cities with a novel deep learning approach

Wangyang Chen[a,b,c], Huiming Huang[a,b,c], Shunyi Liao[a,b,c], Feng Gao[a,b,c], Filip Biljecki[d,e,*]

[a]*Guangzhou Urban Planning & Design Survey Research Institute, Guangzhou, 510060, China*
[b]*Collaborative Innovation Center for Natural Resources Planning and Marine Technology of Guangzhou, Guangzhou, 510060, China*
[c]*Guangdong Enterprise Key Laboratory for Urban Sensing, Monitoring and Early Warning, Guangzhou, 510060, China*
[d]*Department of Architecture, National University of Singapore, Singapore*
[e]*Department of Real Estate, National University of Singapore, Singapore*

Abstract

Urban road networks (URNs) are ubiquitous and essential components of cities. Visually, they present diverse patterns that embody latent planning principles. However, we still lack a global insight into such patterns. In this paper, we propose a scalable deep learning-based framework to automate accurate and multiscale classification of road network patterns in cities and present a comprehensive global implementation on 144 major cities around the world, yielding their multiscale pattern profiles and urban fabrics, highlighting both similarities and contrasts. We observe significant disparities across continents and regions, particularly at larger scales. We give particular attention to exploring inter-city pattern similarities with new metrics we introduce, and uncover subgroups in each continent, unveiling the potential intercontinental dissemination of planning paradigms. We establish four modes of intra-city spatial distribution of patterns considering diversity and clustering. Notably, radial road networks are found to be positively correlated with GDP per capita and negatively correlated with PM2.5 pollution. Our global study provides a new perspective to understand the URN texture of cities, which helps to understand the externalities of different road patterns and accordingly promote scientific and sustainable solutions for urban development.

Keywords: Complex system, Urban science, Street morphology, Street network, Urban analytics

1. Introduction

Urban Road Networks (URNs) are the fundamental infrastructure to support efficient and sustainable urban systems (Maki, 1964; Ganin et al., 2017). They constitute the skeletons of cities and maintain the urban metabolism, which comprises the movement of both human (Frank et al., 2008; Jiang et al., 2009) and freight traffics (SteadieSeifi et al., 2014). Understanding the characteristics of URNs is a perennial topic of interest in urban systems and planning (Bettencourt and West, 2010; Barthélemy, 2011; Barthelemy, 2016). Since URNs are complex systems, portraying their properties is never tractable, always requiring simplification (Lämmer

---

et al., 2006; Strano et al., 2013; Marshall et al., 2018). In this regard, URNs are oftentimes modeled by methods based on graph theories from the perspective of topology (Bafna, 2003; Porta et al., 2006; Cardillo et al., 2006). Various relevant indicators are utilized to embed the original URNs, such as degree of intersections (Kalapala et al., 2006; Masucci et al., 2009), centrality (Crucitti et al., 2006; Kirkley et al., 2018), enclosed block shape (Louf and Barthelemy, 2014), and their combination (Boeing, 2020). While most urban scientists tend to perceive URNs through mathematical methods and quantitative indicators, another, more intuitive and visual-based perspective — the perceptive pattern of URNs — is oftentimes omitted. In this context, a pattern refers to a type of shape that is used to lay out the URNs. It directly manifests the geometry of URNs based on human senses. In the literature hitherto, one of the mainstream taxonomies identifies four categories of street pattern, namely linear, tributary, radial, and grid-iron (Marshall, 2004). Consequently, the interplay between road network patterns and urban mobility (Marshall and Garrick, 2010; Pasha et al., 2016; Wu et al., 2021), social security (Marshall and Garrick, 2011; Rifaat et al., 2011, 2012), and urban vitality (Chen et al., 2021) has been reported in the literature, underscoring the importance of road network patterns in urban systems. However, most preceding studies classify road network patterns manually and do so only in particular geographies (Marshall and Garrick, 2011, 2010; Rifaat et al., 2011), which restricts the scope of study area and thus hinders reliable and comprehensive research at a large scale.

Bridging such gap necessitates developing automatic, scalable, and efficient methods to realize a wide range of road network pattern classifications. A branch of existing methods harnesses spatial features to recognize patterns. Based on the geometry of neighboring blocks, tailor-made algorithms are available to detect gridiron patterns (Yang et al., 2010; Tian et al., 2016). Additionally, radial and linear patterns are also traceable using spatial features of junctions and road segments (Xie and Levinson, 2007; Heinzle et al., 2007). However, these algorithms are only trialed with limited local cases, which are not representative across many different geographies. Their accuracy and stability in a broader scenario are still indeterminate. More recent methods experience a two-step process (He et al., 2017; Wang et al., 2017; Han et al., 2020): establishing a URN indicator set and whereby conducting the classification. Despite a unified way for multiple patterns, the subjectively selected indicators usually oversimplify the intricate URNs, which diminishes the accuracy (Wang et al., 2017). To overcome the obstacles faced by traditional methods, the literature explores to portray the urban form with deep learning technologies (Wang et al., 2023; Li et al., 2023; Wu and Biljecki, 2023). A deep learning framework for road network pattern classification is also proposed (Chen et al., 2021). It takes a graphical input of URNs (Colored Road Hierarchical Diagram — CRHD), which maintains intrinsic geometric properties, and outputs the pattern. Skipping subjective feature engineering, the end-to-end method enables identifying multiple patterns simultaneously with favorable performances.

In the era of big data, urban studies spanning large study areas are gaining momentum to support more insightful and sustainable urban development (Sun et al., 2020; Lemoine-Rodríguez et al., 2020; Boeing, 2022; Biljecki and Chow, 2022; Zhu et al., 2022; Tian et al., 2022; Li et al., 2022; Debray et al., 2023). OpenStreetMap (OSM) lays the foundation for global URN studies, which has been used to explore the history of the global URN sprawl (Barrington-Leigh and Millard-Ball, 2020; Burghardt et al., 2022), and characterize the current URNs around the world with indicator-based methods (Valencia et al., 2019; Boeing, 2022). Nevertheless, the inventory, understanding, and comparison of road network patterns from the visual perspective is still limited to a handful cities (Chen et al., 2021). Here, we substantially expand the state of the art to 144 cities globally, acknowledging the diversity of the most populous cities from all six inhabited continents. These cities have been selected to have a balanced representation of cities around the world with diverse morphological configurations and socioeconomic conditions. Besides dimensional advances among deep learning-based global URN

studies, we also considerably ameliorate the road network pattern classification method. First, the supported categories of road network patterns are enhanced from 4 to 6, with a more universal and computer legible taxonomy integrated by the commonly used ones (Snellen et al., 2002; Marshall, 2004; Southworth and Ben-Joseph, 2013). Second, we consider the scale effect (Openshaw, 1981) on road network patterns, regarding the neglected aspect that patterns vary with scale. Instead of focusing on a monotonous scale, this study introduces a novel approach of multiscale pattern classification that does not only capture how scale mutates the pattern, but also demonstrates continental and dimensional disparities around the world. Furthermore, leveraging the scale-induced variation of road network patterns, we raise the concept, 'pattern convolution', which summarizes the patterns within cities and evaluates inter-city pattern similarities. Based on that approach, we reveal subgroups of cities in each continent, clarifying both internal homogeneity and cross-continental entanglement in road network patterns. We also highlight the intra-city spatial distribution of road network patterns. Through quadrant analysis, we conclude four paradigms of pattern distribution within a city in terms of both proportional and spatial features. Both inter-city and intra-city relationships in road network patterns embody histories of world urban development. We unveil synergies between road network patterns and urban socioeconomic and environmental conditions. Our paper aspires to introduce a new perspective to interpret cities. It allows us to imitate human sense-based urban form classifications on a wide scale. Our global and multiscale study fills the gap in the literature on such topics, which supplements the fundamental materials for high-quality and sustainable urban development and contributes to data-driven urban planning and other domains relying on morphological studies.

2. Methods

2.1. *Urban meshing and multiscale pattern classification*

There are thousands of cities in the world that may be included in such analysis. To keep the analysis feasible and within computational means, we choose major cities around the world as study area, believing that the road network patterns of major cities can represent regional characteristics. We use population as the key criterion to filter major cities. We also highlight the geographic dispersion of selected cities to capture road network characteristics in more regions of the world. Thus, major cities in each continent are filtered separately. After listing the most populous cities on each continent, we further screen the cities considering the diversity of age (new and old cities), locations (inland and coastal cities), and development stages (cities in developed and developing countries), and finally get 144 cities of interest (Supplementary Table 1). For every city of interest, the coordinates of the city center are derived from the World Cities Database maintained by SimpleMaps, which accommodates an up-to-date authoritative database of locations and populations for cities and towns worldwide. Based on a preliminary analysis of the study boundary selection (Supplementary Note 3), we define a consistent study boundary (i.e. a 15 km buffer from the city center) for all the cities, forming a uniform criterion for inter-city comparisons. For multiscale analysis, the study area of each city is meshed into regular grids on small, mid, and large scales with the resolution of 0.5 km, 1 km, and 2 km, respectively. The mid-scale grids comply with the WorldPop 1 km-resolution grids (WorldPop, 2018). Based on the mid-scale grids (actual grids) , we generate small and large-scale grids (virtual grids) with geometric operations. Specifically, each mid-scale grid is split into four small-scale grids, while four adjacent mid-scale grids are combined into a large-scale grid.

We use the Colored Road Hierarchical Diagram (CRHD) to represent the feature of URNs in a grid (Chen et al., 2021). CRHD is a kind of diagram that reflects road hierarchies and structures by lines with different colors and widths (see details in Supplementary Note 1.1). The spatial data of URNs behind it is retrieved from the OpenStreetMap (OSM) database (OpenStreetMap contributors, 2017), queried by the open source Python package OSMnx (Boeing,

2017). CRHDs are generated through a standard workflow (Fig. 1a and Supplementary Note 1.1), which is optimized and released as one of our open source software. We adopt the design of "outreach" to incorporate the interactions with ambient road networks (Supplementary Fig. 1a and Supplementary Note 1.2). The scope covered by a CRHD is referred to as the 'receptive field', and the URNs inside it are seen and classified by the model.
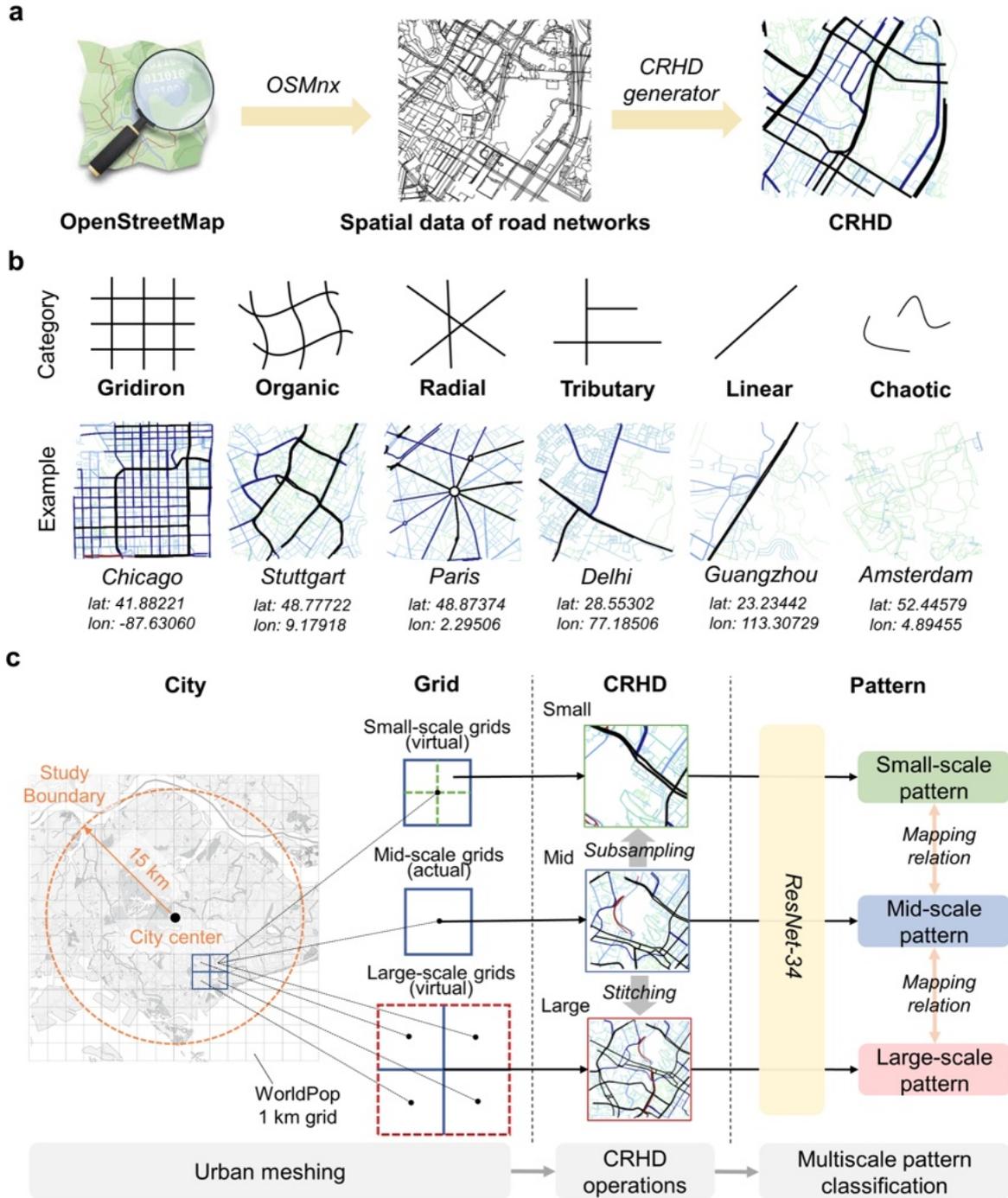
Figure 1: Workflow of urban meshing and multiscale road network pattern classification. **a** The workflow of generating a CRHD from OpenStreetMap (see details in Supplementary Note 1.1). **b** Our taxonomy of road network patterns with example CRHDs (1 km × 1 km). **c** The technical framework of multiscale road network pattern classification for a city (exemplified with Singapore), which consists of three major steps: urban meshing, CRHD operations, and multiscale pattern classification. Source of the raw street network data: (c) OpenStreetMap contributors.

Thanks to the design of actual and virtual grids, we only need to glean mid-scale CRHDs

as the basic materials, with which, CRHDs at other scales can be generated through CRHD operations. We introduce stitching operation for upscaling the CRHD (see details in Supplementary Note 1.3 and Supplementary Fig. 1c). It merges four adjacent mid-scale CRHDs into a large-scale one, by truncating the redundant areas of the input diagrams and concatenating them based on pixel-level matching at the edge. Inversely, subsampling operation splits a mid-scale CRHD into four small-scale ones (see details in Supplementary Note 1.3 and Supplementary Fig. 1d). CRHD operations considerably accelerate multiscale CRHD collection and the following classification.

Next, CRHDs at each scale are classified into different patterns. Considering the global coverage of cities and the fit with our computational method, our pattern taxonomy is supposed to be universally applicable and computer legible. Derived from various commonly used taxonomies (Snellen et al., 2002; Marshall, 2004; Southworth and Ben-Joseph, 2013), radial, organic, gridiron, and no pattern have been proven to meet the above requirements (Chen et al., 2021), We refer to the four categories, while for a more detailed classification, we divide "no pattern" further into three distinctive ones (i.e. tributary, linear, and chaotic). As a result, we obtain six categories with typical visual characteristics: gridiron — densely arranged orthogonal road networks, organic — enclosed major roads with irregular shapes, radial — major/secondary roads spreading out from a central point, tributary — unclosed dendritic major/secondary roads, linear — single linear major/secondary road, and chaotic — road networks lacking major/secondary roads or the aforementioned patterns. The quintessential CRHD for each category is illustrated in Fig. 1b. To conclude, Fig. 1c demonstrates the overall workflow of conducting multiple road network pattern classifications in a city.

2.2. Classification model and performance

ResNets (He et al., 2015, 2016) have been found to be an effective deep learning model for road network pattern classification (Chen et al., 2021). We choose ResNet-34, which performs the best among the ResNets family in our preliminary experiments, as the final model architecture (see details in Supplementary Note. 1.4). The model are trained and tested with a labeled dataset including 1,548 mid-scale CRHDs. CRHDs selected into the dataset must have clear characteristics of one of the six categories and present minimum pattern mixture. Details of training configurations and processes are available in Supplementary Note 2.1. As a classic classification task, the model performance is evaluated with confusion matrix and ROC curves (Supplementary Fig. 2a,b). The results indicate that our model achieves an promising average precision (0.93), recall (0.92), and F1-score (0.92). It performs particularly well in recognizing linear, chaotic, and organic URNs with the accuracy over 0.95, while performs slightly worse for gridiron (0.84), radial (0.88), and tributary (0.88). An explanation for the relative drop in accuracy for these categories is that, aside from their distinctive features, gridiron, radial, tributary, and organic patterns also share some partial similarities that are difficult to completely exclude from the dataset. Nevertheless, considering our model's favorable overall performance and consistent criteria for handling the difficult-to-distinguish cases, the flaw is quite acceptable and should not significantly affect the results. We also validate the performance at other scales through cross-scale experiments (Supplementary Note 2.2). Therefore, the model is reliable enough for this study.

2.3. Pattern Diversity Index

Pattern Diversity Index (PDI) is defined to delineate the diversity of road network patterns within a city. For a city, the larger the PDI value, the more dispersed and uniform the proportion of different road network patterns. PDI is calculated by the formula of Shannon entropy (Shannon, 1948) given the pattern proportions at a certain scale:

$$PDI = -\sum_{i=1}^{n} p_i \log p_i \tag{1}$$

where n denotes the total number of pattern categories in the city, and p_i is the proportion of the ith category. Mathematically, the minimal PDI is 0 when all the grids in the city belong to an identical category. The maximal PDI is $-ln(1/6)$ (≈ 1.792) when the proportions of the six categories are evenly distributed.

2.4. Neighborhood Similarity Index

Neighborhood Similarity Index (NSI) is proposed to quantify the level of pattern spatial clustering in an area or a city. We refer to the widespread indicator of spatial autocorrelation (Moran's I) (Moran, 1950; Anselin, 1995), and extrapolate the definition of NSI as the similarity level of road network patterns between proximal grids. Akin to spatial autocorrelation, NSI has both global and local versions as well. Global NSI (GNSI) summarizes neighborhood pattern similarities at the city level, which is measured by the quotient of the total number of neighboring grid pairs with consistent patterns and the total number of neighboring grid pairs in the city (Eq. 2). Local NSI (LNSI) reflects the level of pattern similarity for a specific grid cell, which is measured by the quotient of the number of neighboring grids with the same pattern as the grid and the total number of neighbors of the grid (Eq. 3). The neighbors of a grid are determined by Queen's contiguity.

$$Local\ NSI(g) = \frac{\sum\limits_{n \in N(g)} \mathbb{I}(p(g) = p(n))}{|N(g)|} \tag{2}$$

$$Global\ NSI(c) = \frac{\sum\limits_{g \in G(c)} \sum\limits_{n \in N(g)} \mathbb{I}(p(g) = p(n))}{\sum\limits_{g \in G(c)} |N(g)|} \tag{3}$$

where g denotes a grid, $N(g)$ is the neighbor set of grid g, $|\cdot|$ denotes the number of elements in set $\cdot$, and n represents a neighbor. $p(\cdot)$ represents the road network pattern of grid $\cdot$. $\mathbb{I}(\cdot)$ is the indicator function which returns 1 if condition $\cdot$ is true and returns 0 otherwise. c is a city and $G(c)$ denotes the grid set of city c.

3. Results

3.1. Scale effect on road network patterns

The road network pattern in a fixed location and time can vary at different scales of receptive fields. Thus, we firstly conduct some experiments to investigate the scale effect on road network patterns. Note that, instead of distinguishing road network patterns of streets with different service levels (Marshall, 2004; Marshall and Garrick, 2010, 2011), which is characterized by a dramatic scale shift from the neighborhood to the citywide level, we focus on road network patterns formed by all road grades. In our case, the scale effect can be portrayed by the scale-induced variation in predictive probabilities (Fig. 2a). Specifically, we regard the mid-scale (1 km radius) road network pattern as the prior category of a location classified at the original scale. Then we classify the pattern of the same location for multiple times with varying radii and record the variation of predictive probabilities for each category. The average variation of probabilities across the test set for each prior category is shown in Fig. 2b. The scale effect on different prior categories appears to be heterogeneous. Gridiron pattern becomes more evident during upscaling, which is unique compared with the counterparts. For patterns with less major road components such as linear and chaotic, downscaling casts an insignificant impact on their
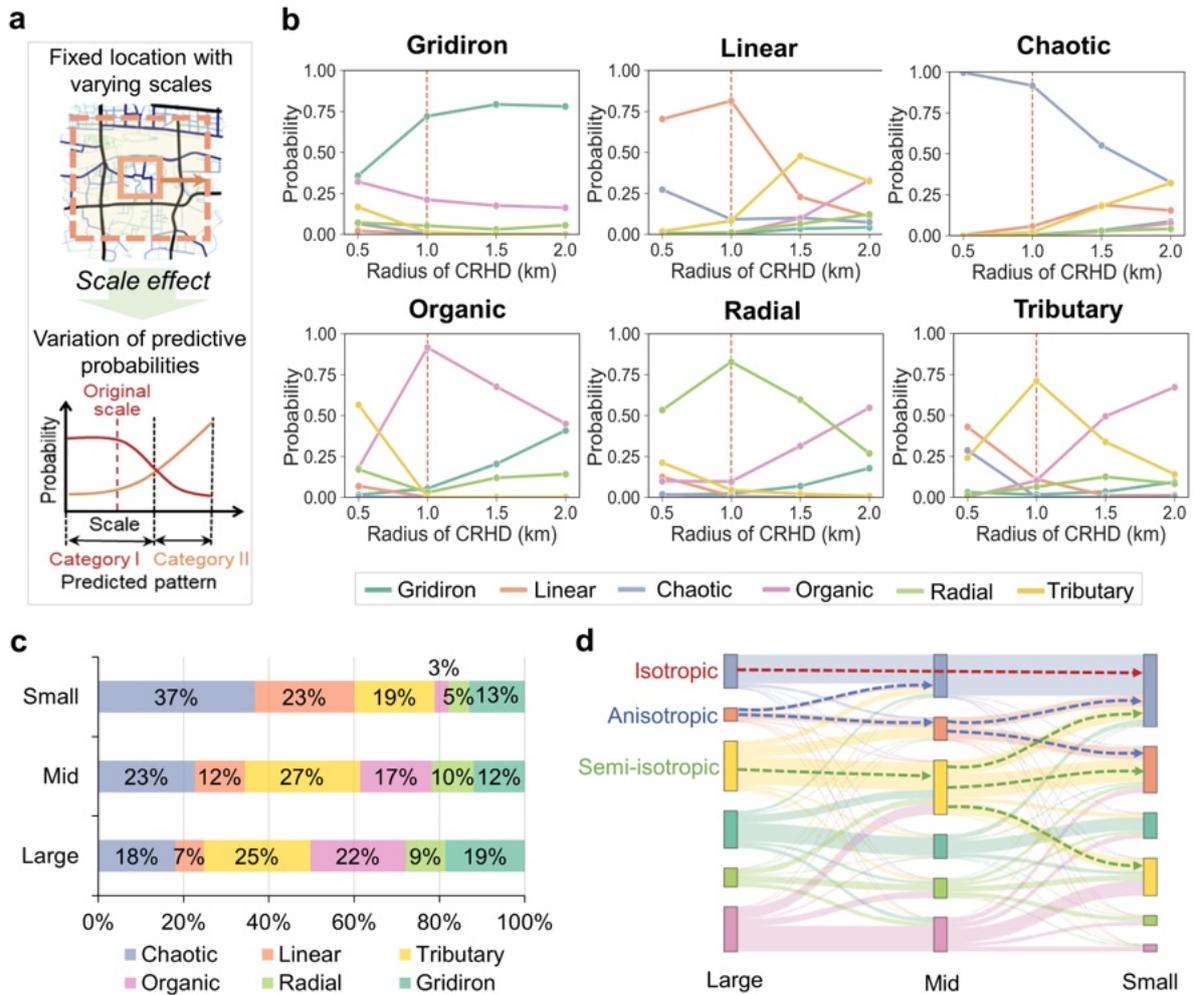
6

Figure 2: Scale effect on road network patterns. **a** The mechanism for evaluating the scale effect on road network patterns. **b** Scale-induced variations of predictive probabilities for each prior category. **c** Global pattern proportions at different scales. The global proportion of a pattern is the amount of grids pertaining to the pattern divided by the total amount of grids of all cities. **d** Global cross-scale mapping relations. There are two layers of mapping relations among the three scales, which are visualized by the Sankey diagram. The height of a node (i.e. pattern) denotes its proportion at the scale, while the width of a link indicates the proportion of aggregated cross-scale mapping relations from the larger scale to the smaller one (see detailed statistics in Supplementary Table 5).

recognition. However, when more adjacent streets are encompassed into the receptive field due to upscaling, these two patterns evolve into more complex patterns (linear towards tributary and organic, and chaotic towards linear and tributary), indicating a presumable transferring chain from simple to complex patterns. Conversely, we can also observe the inverse conversion from organic and tributary to those simpler patterns when the scale shrinks. As a relatively isolated case, radial tends to transfer towards organic with more newly formed road circuits during upscaling, while it remains robust in the opposite direction.

Following the framework in Fig. 1c, we adopt multiscale road network pattern classifications in our cities of interest. The results uncover heterogeneities in proportions of patterns at different scales (Fig. 2c). At small scale, 79% of URNs within our study area are of simple pattern such as tributary, linear, and chaotic. When the scale expands to mid and large, the shares of linear and chaotic URNs shrink dramatically, which are mainly replaced by organic and radial URNs. Besides, tributary is a widespread pattern with a considerable proportion (around a quarter) at all scales. Although not as prevailing as tributary, gridiron is also a common pattern that occupies over 10% of the urban area regardless of the scale.

We leverage mapping relations across the scales to explore how larger-scale patterns are

7

constituted by smaller-scale patterns (Fig. 2d). We observe three general constitutive types: isotropic, semi-isotropic, and anisotropic. If links running though the same category are continuously strong across the scales, it indicates that the pattern is self-repetitive, which we consider as isotropic. Gridiron and chaotic are typical isotropic patterns. In contrast, linear and radial exhibit the opposite feature, which is anisotropic. URNs of these categories are oftentimes composed of various subpatterns. For example, linear is mainly made of linear and chaotic subnetworks, while radial is associated with even more subpatterns. Another constitutive type that lies between is semi-isotropic, represented by tributary and organic. Semi-isotropic patterns exhibit an isotropic property from large to mid scale but transition into anisotropic from mid to scale scale. For instance, large-scale tributary URNs are mainly constituted by mid-scale tributary URNs, but the subpatterns of mid-scale tributary URNs become far more diverse.

3.2. Continental and dimensional comparison of dominant patterns

After studying the general proportion of road network patterns over the globe, we explore the similarities and disparities of multiscale patterns across different cities and regions. For each city, the pattern that accounts for the largest proportion at a scale is considered as its dominant pattern at that scale, and the proportion of the dominant pattern (PDP) reflects the significance of dominance. We present global landscapes of multiscale pattern dominance.

At small scale, the distribution of dominant patterns among cities appears to be somewhat monotonous (Fig. 3a), with over half (58%) of the cities dominated by chaotic (colored by purple). Most of these cities are located in South America, Europe, and especially Africa where all the cities are dominated by chaotic (Fig. 3b). It is noted that Chinese cities are primarily dominated by linear URNs, while most North American cities exhibit gridiron-dominant. At small scale, the receptive field of a CRHD covers several contiguous blocks, and most contributors of the pattern serve neighborhood-level traffics. Local urban areas without sufficient neighborhood roads tend to be classified as chaotic. Thus, for chaotic-dominant cities, the higher their PDPs, the more likely they are deficient in neighborhood connectors. Meanwhile, for cities dominated by other patterns, those with more complex dominant patterns tend to possess more adequate neighborhood connectors. The observation that all leading gridiron-dominated cities come from North America (Fig. 3c) uncovers the advantage of North American cities in neighborhood mobility. Many other developed Western cities, headed by London, Toronto and Paris, show the dominance of less complex pattern, i.e. tributary. Chinese cities occupy high-ranking positions of the linear pattern. The leading chaotic-dominated cities are mostly from the underdeveloped world. To some degree, the small-scale dominant patterns are related to the status of urbanization around the world.

When the scale shifts from small to mid, visible changes occur on the distribution map (Fig. 3d). At middle scale, considering the existence of outreaches, a few regional connectors become contributory to the pattern, together with the neighborhood roads. As a result, some chaotic areas at small scale are supplemented by the surrounding URNs and present clear patterns. In total, 72% of cities of interest exhibit dominance of clear pattern at mid scale (Fig. 3e), while the rate at small scale is only 42%. Tributary becomes the most prevailing dominant pattern around the world, taking over the position of chaotic. The conversion is particularly significant in Europe, where 20 out of the 34 small-scale chaotic-dominant cities become pattern-dominant at mid scale. Exceptionally, the two largest cities, London and Paris, are dominated by organic. It can be attributed to their denser road networks and larger downtown areas with abundant road infrastructures. The majority of Chinese cities are also tributary-dominant at mid scale. Similarly, major eastern coastal cities, such as Hangzhou and Shanghai, have more organic URNs than other cities in China. Regarding organic dominance, Mexico City and Tehran rank as the top 2 cities (Fig. 3f). The preference to gridiron in North America preserves at mid scale, with U.S. cities sweeping the top 5 positions of gridiron PDP. Particularly, the gridiron
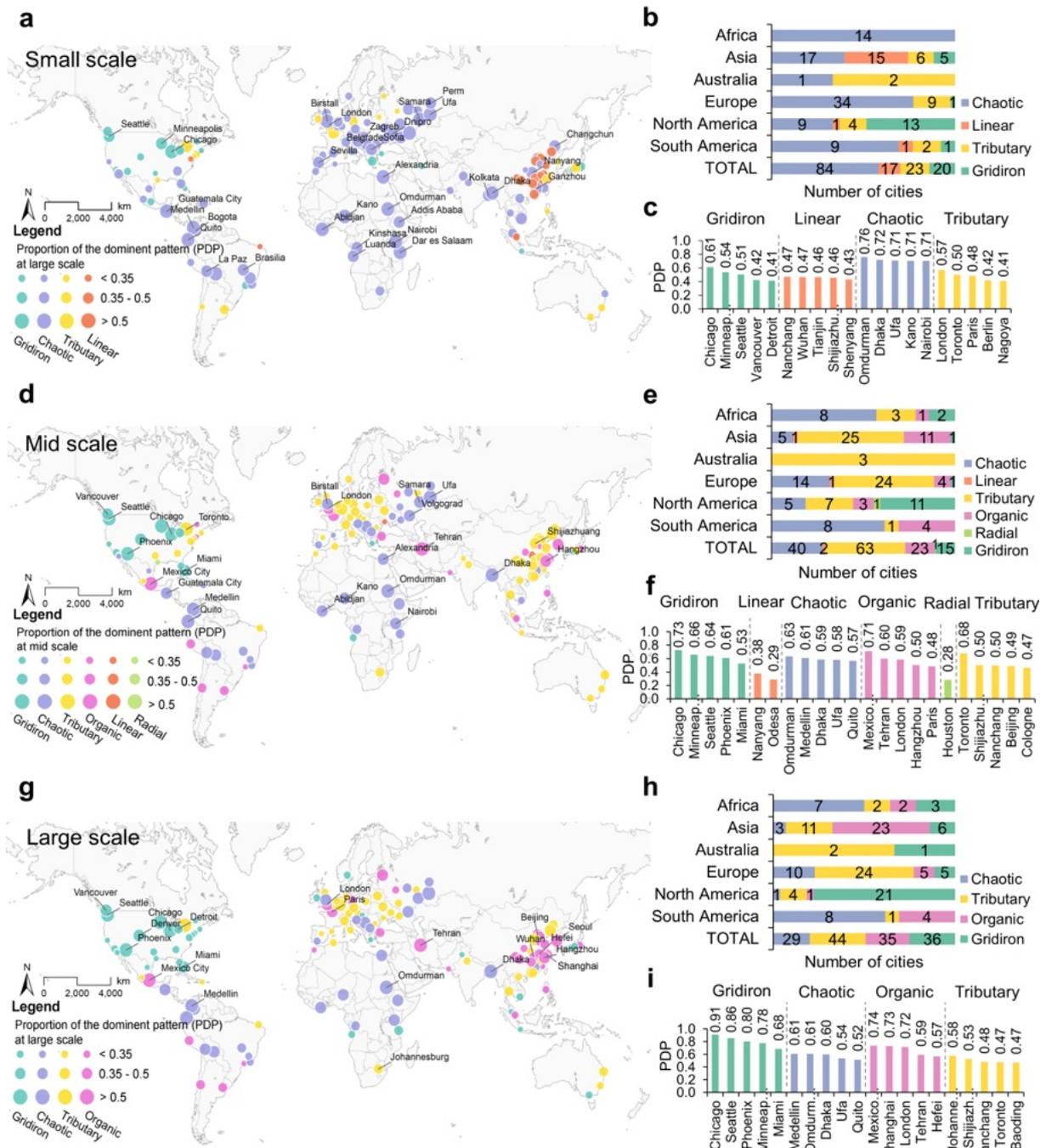
Figure 3: Continental and dimensional heterogeneities of dominant patterns. Distribution of cities with dominant patterns and proportions of the dominant pattern (PDPs) at different scales: **a** small, **d** mid, and **g** large. Each point on the world map represents a city whose color and size denote the dominant pattern and the PDP of the city, respectively. The larger the point, the higher the proportion of the dominant category. Cities with PDP above 0.5 are labeled with their names. PDP values for individual cities at all scales could be found in Supplementary Table 6. Zoomed-in maps for regions with dense cities of interest are available in Supplementary Fig. 4. The number of cities of each dominant pattern group for each continent at different scales: **b** small, **d** mid, and **f** large. **c**, **f**, and **i** display cities with the top 5 PDP in each dominant pattern group. In some cases, the number of cities dominated by some patterns is less than five.

PDPs of Phoenix and Miami grow dramatically from small scale. In contrast, cities on the East Coast of the U.S. are dominated by tributary, but their PDPs are basically below 0.35, indicating a considerable mixture of different patterns. Note that chaotic remains the primary pattern for South American and African cities, although some cities such as Johannesburg and Lima are no longer in the list. The dominance of linear and radial is relatively scarce at mid scale, with only three cities falling into these groups with low PDPs.

At large scale, regional URNs become the principal determinants of road network patterns, diminishing the impact of small chaotic areas on the overall pattern. The intercontinental disparity in patterns is the most significant at this scale. Geographically, we identify four major clusters with distinct dominant patterns (Fig. 3g), including East Asia, Europe, North America, and South America & Africa, respectively. The pattern commonality witnessed in China at smaller scales extends to other parts of East Asia, where most cities are organic-dominant. This cluster includes large East Asian metropolises (e.g. Shanghai, Hangzhou, Seoul, etc.), as well as some Southeast Asian cities (Singapore and Manila) which are influenced by Chinese culture. In Europe, most cities are characterized by a tributary dominance, with a few exceptions such as London and Paris. The prevalence of tributary is consistent across most of Europe and even spreads to Australia, which shares similar cultural roots. For North American cities (mainly those from the U.S. and Canada), gridiron is unsurprisingly the predominant pattern at large scale (Fig. 3h). Compared with mid scale, most cities on the East Coast of the U.S. transfer from the dominance of tributary to gridiron, resulting in a more unified gridiron dominance in the continent. Over 90% of the large-scale URNs in Chicago are gridiron, followed by Seattle and Phoenix (Fig. 3i). In the last cluster, half of the cities in South America and Africa are dominated by chaotic. Some cities are chaotic-prevalent across all scales. This could be attributed not only to the possible underdevelopment of road infrastructures, but also to the smaller urban area resulting from the lagged urban expansion behind urban population growth in these continents (Sun et al., 2020). With a consistent study boundary for all cities, smaller urban areas entail the inclusion of less urban suburbs into account, leading to biases in the proportion of chaotic URNs.

3.3. Panoramic pattern profile and inter-city similarity

The pattern dominance reflects the majority of road network patterns in a city, but overlooks the composition of other patterns. To provide a comprehensive view of multiscale road network patterns, we utilize rose diagrams to visualize continental profiles (Fig. 4a), which reveal additional findings that may be overshadowed by the dominant pattern analysis. For example, Africa and South America are akin in the dominance pattern (mainly chaotic). However, the profiles indicate that tributary is the secondary pattern in Africa at all scales, while organic is more prevailing in South America, especially at large scale. Globally, radial is found to be the rarest pattern regardless of scales and continents. Howver, it is a distinct pattern that should not be overlooked, and it may be present in core districts of cities such as London and Paris. Meanwhile, some findings are reinforced by the profiles. For example, tributary and organic appear to be the principal components of the urban fabric in Asia. In North America, significant dominance of gridiron pattern is observed at all scales, confirming a well-known fact but hitherto not established through such approach.

Besides the intuitive visualization of pattern profiles, we also use summary indicators to encapsulate the characteristics. Supplementing the dominant pattern and PDP, we introduce Pattern Diversity Index (PDI) to quantify the diversity of patterns in a city. A larger PDI value implies a more diverse combination of road network patterns in the city, and vice-versa. For all the cities, PDIs are calculated independently at each scale. In general, road network patterns exhibit the highest degree of diversity at mid scale (median PDI = 1.51), compared with that of small scale (median PDI = 1.41) and large scale (median PDI = 1.47). To understand the
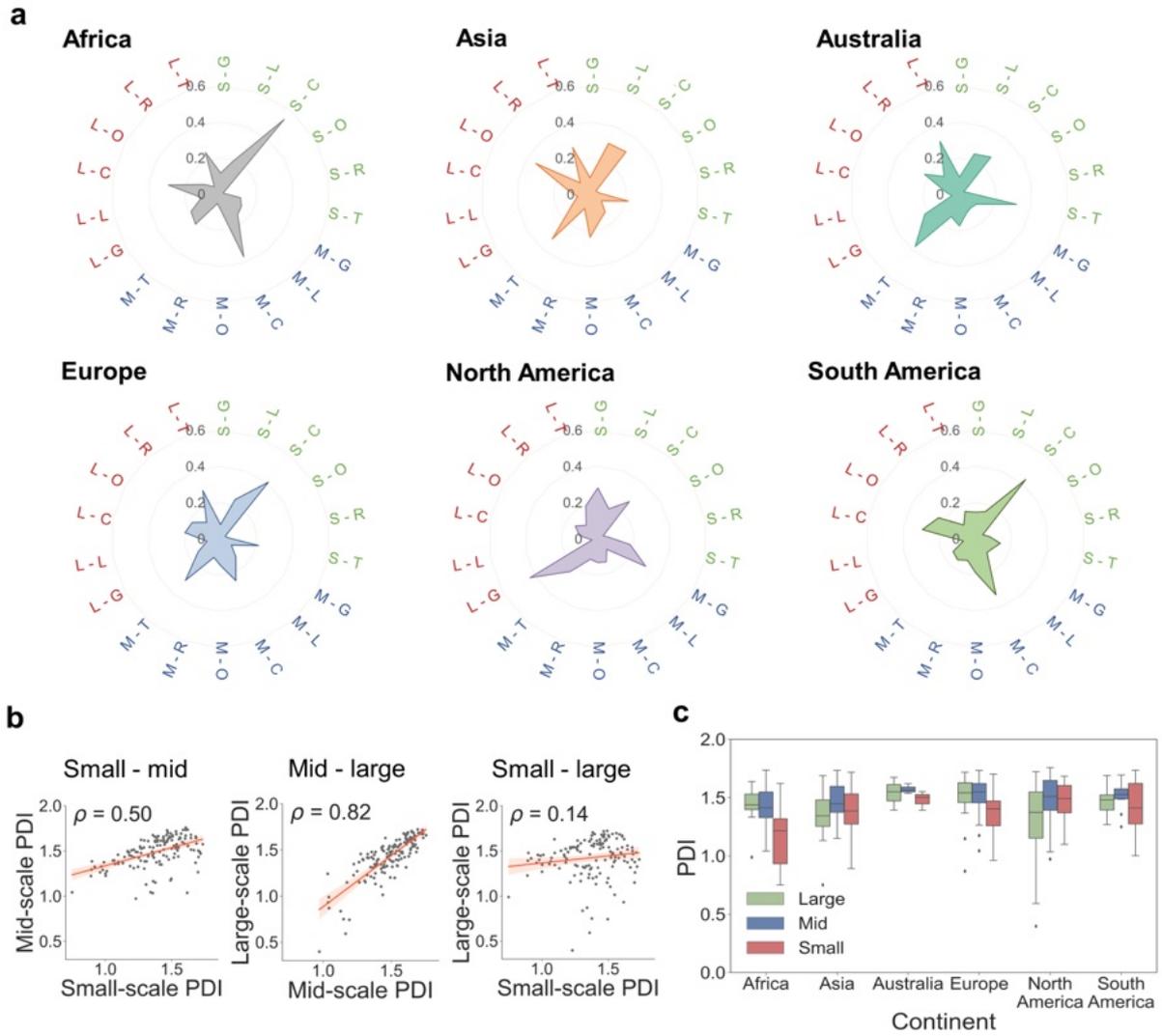
Figure 4: Panoramic pattern profiles and pattern diversities. **a** Continental panoramic profiles of road network patterns, presented by rose diagrams indicating the continentally average pattern proportions at every scale. To explain the abbreviated annotations, the character before the dash denotes the scale (small as S, mid as M, and large as L), while the one after the dash denotes the pattern (gridiron as G, linear as L, chaotic as C, organic as O, radial as R, tributary as T). **b** Pairwise correlations among the PDIs at different scales measured by Pearson correlation coefficients (ρ). **c** Box-plots showing the varying distributions of PDIs across the scales in each continent. PDI values for individual cities at all scales could be found in Supplementary Table 6.

cross-scale association of pattern diversity, we examine the pairwise correlations among the PDIs at multiple scales (Fig. 4b). There is a strong synergy between the mid-scale and large-scale PDIs ($\rho = 0.82$), which is followed by the moderate correlation between small-scale and mid-scale PDIs ($\rho = 0.50$). However, the small-large correlation ($\rho = 0.02$) is not significant. It hints that the interplay of pattern diversity between contiguous scales is more prominent than that between separate scales. Moreover, the greater uncertainty of patterns at small scale presumably weakens the association between small-scale PDI and its counterparts.

The PDI distributions of cities on each continent and the variations induced by scale are illustrated in (Fig. 4c). For Africa, the small-scale PDIs are significantly smaller than the rest of the world. It may be due to the outstanding proportion of chaotic URNs. As the scale increases, their larger-scale PDIs approach the global average level. Similarly, Australia and Europe also present lower pattern diversity at small scale. However, their variances within the continent are less notable than Africa. London and Paris stand out as outliers with considerably lower PDIs at mid and large scale within Europe again. In contrast, North America exhibits an opposite trend

regarding the variation in PDI distributions across different scales. Generally, North American cities have the least diverse road network patterns at large scale, in accordance with their high gridiron PDPs (Fig. 3i). In addition, when projecting the PDIs onto maps, disparities within the continents become evident (Supplementary Fig. 5). In North America, coastal cities are more diversely patterned than the inland ones. In Asia, the pattern diversity of Chinese cities keeps low at all scales, while South and Southeast Asian cities surpass the median level. These two groups of cities strike a balance, resulting in a relatively neutral pattern diversity statistics in Asia.
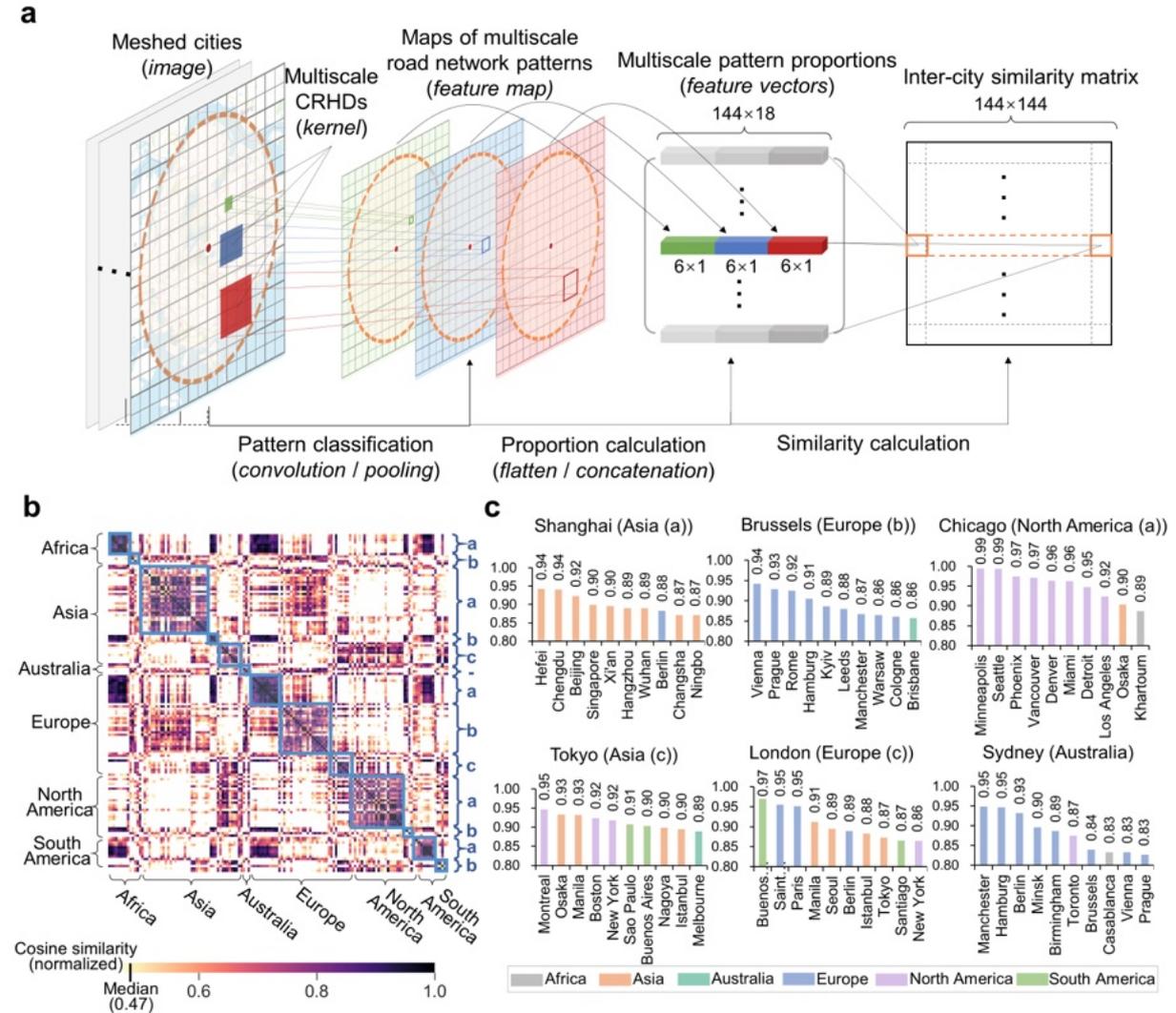
Figure 5: Pattern convolution and inter-city pattern similarity. **a** The conceptual and schematic process of pattern convolution. The method refers to the architecture of a naive inception module (Szegedy et al., 2015), where multiscale CRHDs correspond to the kernels with different sizes (or receptive fields) and pattern maps resemble the feature maps, which are flattened and concatenated by proportion calculation at the next stage. The obtained pattern proportions serve as an embedding of city-level URN characteristics. **b** Inter-city pattern similarity matrix. The inter-city pattern similarity is gauged by the normalized cosine similarity (0-1) between their pattern proportions. The matrix here is a concise version that briefly shows the subgroups (blue squares on the diagonal, labeled in alphabet sequence on the right) within each continent (Australia only has one subgroup so it is not annotated by letters). Only the cells with the similarity score above the median (0.47) are visualized. The high-resolution matrix with more descriptions is available in Supplementary Fig. 6. **c** Typical cities in different subgroups with their top 10 similar cities (ranked by similarity scores). We use different colors to mark the continents that the similar cities come from.

Now that we have obtained the multiscale pattern proportions of our cities of interest, we continue to explore the inter-city similarities. Our framework of multiscale pattern classifica-

12

tion (Fig. 1c) could be seen as a convolution process acting on meshed cities. We term the process 'pattern convolution' (Fig. 5a), which encodes road network patterns within a city into pattern proportions. Using these 18-dimensional vectors, we evaluate the inter-city similarity and obtain a 144 × 144 pattern similarity matrix (Fig. 5b). This matrix divides cities into subgroups in each continent, and also reveals intercontinental associations. Totally, thirteen subgroups are detected across the six continents. To give a succinct but representative interpretation of the results, we pick out six typical subgroups and a representative city from each subgroup respectively, along with their top 10 most similar cities worldwide (Fig. 5c). Our first observation is that most Chinese cities form a subgroup themselves (Asia (a)). In this group, we could find Shanghai, which is probably the Chinese city bearing the most western heritage. However, its road network patterns are more identical to other Chinese cities. Singapore, as a city influenced by Chinese culture, is also found in this subgroup. In contrast, Tokyo in Japan pertains to another subgroup in Asia (Asia (c)), which shows evident connections with western cities. This subgroup also includes other cities linked closer to the west, such as Osaka, Seoul, and Istanbul. In Europe, cities seem to be partitioned in terms of their international influence in the history. Cities in Europe (b), represented by Brussels, exhibit strong internal similarity with most European cities, except for those dominated by chaotic (Europe (a)). It is interesting that Europe (b) turns out to resemble Asia (a) moderately, indicating a potential entanglement of street patterns between the oldest and newest urbanized area in the world. Europe (c) consists of European cities with greater international influence, such as London, Paris, and Madrid. These cities take a role in the world colonial history, and exert profound influence on relevant regions. London, as a typical example, shares remarkably similar road network patterns with cities in Asia, Australia, South America, and North America. North America (a) is another subgroup characterized by general homogeneity within the continent. Cities in this subgroup are mostly gridiron-dominated cities in the U.S. and Canada. Furthermore, the close morphological relationship between Australian and European cities is verified again, considering that 8 out of 10 most similar cities to Sydney are in Europe. Sydney is also a suitable case for investigating the effect of topography on inter-city pattern similarities. It is characterized by an organic city core intermingled with a few gridiron or radial patterns and broad tributary residential zones. One typical topography is a broad waterbody (Sydney Harbor) near the city center, which is classified as chaotic. The cities that are most similar to Sydney, as identified by our method, not only share analogous road network patterns. Some of them even have similar topographic conditions (e.g. Hamburg and Toronto). This finding suggests that the road network patterns of some cities may be shaped by a combination of cultural and topographical influences, and our method can capture this information to some extent.

3.4. Intra-city spatial distribution of road network patterns

Intra-city spatial distribution of road network patterns is also an interesting topic to investigate. For simplicity, we concentrate on mid-scale patterns in this section. We emphasize the spatial clustering of road network patterns, considering that spatial clusters of different urban forms could reflect urban histories and planning ordinances (Ortman et al., 2014; Xue et al., 2022). We propose a indicator, Neighborhood Similarity Index (NSI), to quantify the level of pattern clustering in a city or a local area, using global NSI (GNSI) and local NSI (LNSI), respectively. In Fig. 6a, we illustrate the distribution of cities with mid-scale GNSIs globally. European cities constitute a geographic group with a low-level pattern clustering. This group also includes the cities on the East Coast of North and South America, Southeast Asia, and Australia, which happen to be the major European colonial territories in and before the 19th century. It supports the transplant of western-style urban form in colonial urban development (King, 2012). Cities with high GNSIs are subject to different indigenous conditions. Compared with the earlier built cities on the east coast, U.S. Midwest cities have more regular and contin-

uous URNs under the zoning ordinance enacted in the early 20th century (Whittemore, 2012). Besides, since most urban areas in China are developed in post-reform period with corporate planning paradigms (Ma, 2002; Wu et al., 2006), their road network patterns are more uniform. In Africa, the high GNSIs can root from the large number of unbuilt suburbs within the study boundary.
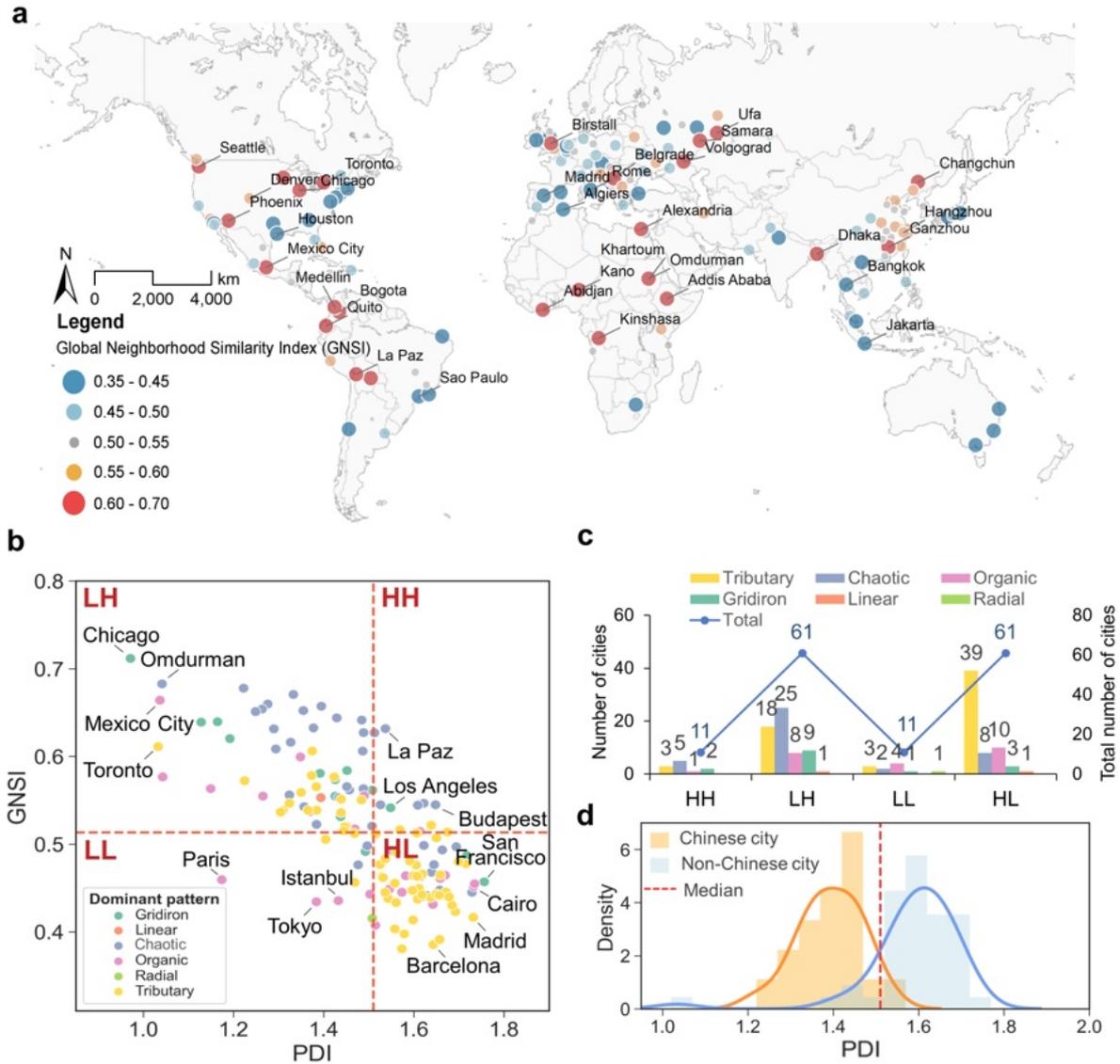
Figure 6: Modes of intra-city spatial distributions of road network patterns. **a** The distribution of cities with midscale GNSIs. The color of the point indicates the absolute value of GNSI, while the size of the point represents the level of deviation from the median. GNSIs for individual cities could be found in Supplementary Table 6. **b** Scatter-plot between PDIs and GNSIs for cities of interest. The color of the point indicates the dominant pattern of the city. The red dashed lines mark the median of each axis, which divide the feature space into four quadrants: namely High-High (HH), Low-High(LH), Low-Low (LL), and High-Low (HL). **c** Bars indicate the number of cities with different dominant patterns in each quadrant, while the blue line is the total amount of cities of interest in each quadrant. **d** PDI distribution density curves of tributary-dominated Chinese and non-Chinese cities. The red dashed line indicates the median PDI of all cities of interest.

To integrate both proportional and spatial knowledge, we conduct a cross-analysis among the pattern indicators. We preliminarily investigate the distributions of individual indicators and their pairwise correlations (Supplementary Fig. 7). PDI and PDP follow a unimodal distribution (skew normal distribution), while GNSI follows a multimodal distribution, implying different modes of pattern clustering among the cities. As expected, PDP and PDI have a strong negative correlation (ρ = -0.88) because of their shared reflection on pattern proportions. Al-

14

though GNSI is also partly associated with pattern proportions, its spatial characterization is indispensible. Thus, we choose the indicator less correlated with GNSI — PDI, as the final proxy of proportional features. Consequently, we disperse the cities into the feature space defined by PDI and GNSI (Fig. 6b). The space is partitioned into four quadrants by the median of each coordinate. An immediate finding is that most cities fall in the LH and HL quadrants, which conforms the overall trend that rising pattern diversity reduces the likelihood of pattern clustering. Nevertheless, some cities still lie in the rest two quadrants.

Some potential relationships between quadrant groups and dominant patterns are observed. Over 90% of tributary-dominated cities fall in the LH and HL groups with a higher concentration in the latter (Fig. 6c). We notice that cities in these two groups actually belong to distinct regions. Tributary-dominated cities in the LH group mostly come from China, while the majority of those in the HL group do not. The distinction is evident in their PDI distribution density curves (Fig. 6d), which are well separated by the median PDI of all cities. It reminds us that although we perceive similarities between Chinese cities and a subgroup of European cities through pattern convolution, there are still disparities in their spatial distributions of patterns. Tributary URNs are more prevalent in Chinese cities than in European ones. We also find that 25 out of 40 chaotic-dominated cities belong to the LH group, and over half of the gridiron-dominated cities is in the same group. These findings stress the necessity of considering spatial perspectives when interpreting street patterns of cities.
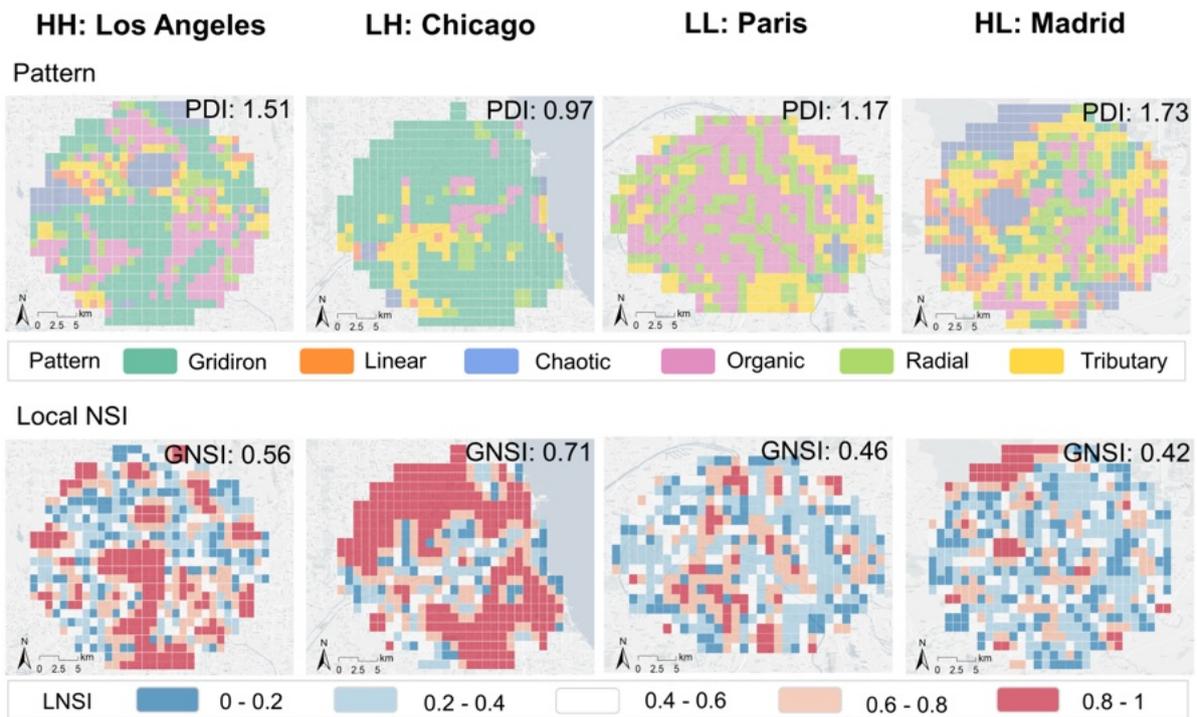
Figure 7: Road network pattern and LNSI maps for representative cities in each quadrant.

Fig. 7 displays the pattern and LNSI map of a representative city from each quadrant (more example cities available in Supplementary Fig. 8). LNSIs successfully capture the spatial clusters of road network patterns in cities. As an example high in both pattern diversity and clustering (HH), Los Angeles contains multiple spatial clusters with different patterns. The organic cluster in the southeast is the early settlement before the enactment of the zoning ordinance (Whittemore, 2012), while the gridiron clusters in the mid and south are built afterwards. In comparison, LH cities have less diverse patterns and thus embody a higher level of neighborhood similarity. Chicago is a typical LH city almost entirely covered by gridiron URNs, with the exception of the canal areas. Similar features also present in cities dominated by other pat-

terns such as organic (Mexico City), tributary (Toronto) (Supplementary Fig. 8). In LL cities, the dominant patterns also occupy a large proportion of URNs, but they are not fully gathered. For instance, in Paris, organic is the dominant pattern, but radial URNs scattered are among the organic ones, lowering down both the GNSI and LNSI of the city. Lastly, HL cities (e.g. Madrid) show a limited pattern clustering similar to LL cities. However, the difference is that they bear a blending of manifold patterns within the city.

3.4.1. Synergy with urban socioeconomic and environmental conditions

Road networks serve as the fundamental infrastructure for urban socioeconomic activities. Their patterns may affect the efficiency of urban systems, thereby being potentially related to socioeconomic and environmental conditions. To simply verify this effect with our results, we conduct some straightforward correlation analyses. Due to the lack of a global database for city economic indicators (e.g. GDP, GNI, etc.), we leverage country-level GDP, GDP per capita, and GNI per capita from World Bank as proxies. The city-level socioeconomic vitality is reflected by the average PP-VIIRS-like nighttime light (NTL) brightness in 2020 (Chen et al., 2020). Population growth are measured by the growth rate of population estimated by World-Pop within the 15 km city boundary from 2010 to 2020. In addition, we also account for the negative environmental externalities of cities with annual PM2.5 pollution data from WHO Air Quality Database. To make the investigation concise and clear, we use the pattern indicators at the most representative scale (mid scale) to represent city-level road network patterns, and obtain the Pearson correlation matrix between the pattern indicators and the aforementioned socioeconomic and environmental indicators (Supplementary Table 7).

The degree of economic development, as measured by GDP per capita and GNI per capita, presents a significant positive correlation with the proportion of gridiron and radial URNs ($\rho > 0.4$, $p < 0.05$). However, the impact of the proportion of gridiron URNs weakens if we exclude the U.S. cities characterized by gridiron-dominated URNs and developed economies, while the positive correlation remains for radial (Supplementary Table 8). Gridiron and radial URNs often signifies greater investment in road network planning and construction, which is expected to improve urban mobility and promote economic development. The finding also suggests that gridiron road network may not be a general planning paradigm for achieving economic prosperity outside the U.S. Radial URNs show more consistent ties to more developed economies. In contrast, the shortage of systematically planned road networks may symbolize and exacerbate economic underdevelopment, given that the proportions of linear and chaotic URNs are negatively correlated with the economic indicators ($\rho < -0.35$, $p < 0.05$). Cities with higher GDP/GNI per capita are correlated with a more mixed spatial distribution of road network patterns, indicated by a smaller GNSI).

Cities with a higher proportion of gridiron, radial, and organic URNs are associated with greater average NTL brightness than those with more tributary, linear, and chaotic URNs. Since NTL brightness is a common proxy of economic vitality, the findings reinforce the potential connection between well-established URNs and advanced economies reflected by economic indicators.

Another observation is that a higher proportion of organic ($\rho = 0.454$, $p < 0.05$) and radial ($\rho = 0.242$, $p < 0.05$) URNs is associated with more population. The positive correlation remains significant (organic: $\rho = 0.469$, $p < 0.05$; radial: $\rho = 0.334$, $p < 0.05$) even when excluding all the Chinese cities, which generally have both more organic URNs and population (Supplementary Table 9). This indicates that organic may be conducive to accommodating larger populations. Besides, population growth is positively correlated with the proportion of chaotic URNs ($\rho = 0.202$, $p < 0.05$), indicating that cities retaining more areas with irregular URNs (e.g. urban villages and slums) may experience faster population growth.

Furthermore, cities with more linear URNs are correlated with higher levels of PM2.5 pol-

lution, while those with more radial URNs show the opposite trend. Although local industry is often the main contributor to air pollution, road network patterns may also affect road traffic pollution. Cities with more linear URNs may be subject to overall worse mobility, resulting in increased vehicle detours and aggravated air pollution. In contrast, radial URNs provide greater flexibility in terms of road connectivity, which may be beneficial to reducing driving distances and mitigating air pollution.

4. Discussion

The contribution of this work is three-fold. First, this study sheds light on visual-based road network patterns around the world with fine spatial granularity and introduces a scalable deep learning framework that can accommodate more cities in the future. The framework is also affiliated with a comprehensive toolkit, from pattern indicators (e.g. PDP, PDI, and NSI) to detailed feature extractors (e.g. pattern convolution), which greatly facilitate the study of urban morphology in various scenarios. Second, our study establishes an inventory of road network patterns covering primary urban areas worldwide. As a feature that reflects the sophistication, efficiency, and externalities of urban systems, road network patterns can be integrated into broad research fields. For example, we find that the proportion of radial URNs may be an indicator of urban economic development and air quality conditions, and organic road patterns are associated with accommodating more population. The interplay could be portrayed further by incorporating our results with neighborhood attribute estimations (Dong et al., 2019; Gebru et al., 2017). Furthermore, our methods can also be used to monitor the progress and quality of urban expansion (Barrington-Leigh and Millard-Ball, 2020; Xu et al., 2020), gauge the environmental impact of urban morphology, including urban climate (Xu et al., 2017; He et al., 2020), carbon emissions (Duren and Miller, 2012; Van Houtan et al., 2021; Deng et al., 2023), and air quality (Huang et al., 2022). The existing and prospective results are valuable materials for guiding rational urbanization (Zhu et al., 2022; Sun et al., 2020; Elmqvist et al., 2013) and sustainable urban development (Burke et al., 2021; Elmqvist et al., 2019; Patias et al., 2021), especially for the cities in the developing world to learn from the pioneer cities. Third, our image-based representation of URNs and deep learning-based approach open up new directions for urban morphology studies. This study reveals promising accuracy of deep neural networks in urban form classification. Our proposed method, pattern convolution, effectively summarizes city-level URN characteristics with the simplest aggregation of pattern maps using pattern proportions. These findings unveil the potential of using computer vision techniques to capture visual features of the built environment, such as street canyons (Middel et al., 2019; Ito and Biljecki, 2021) and building footprints (Wu and Biljecki, 2022, 2023). Based on the powerful fitting ability and massive training cases, artificial intelligence techniques may incubate urban morphology theories with stronger predictive capacities, which are oftentimes limited in traditional case studies (Moudon, 1997). Such advances can support next-generation studies on urban planning and computing.

The findings of this study have to be seen in light of the following limitations. There are still some unconsidered factors in our city selection strategy that might affect the results. For example, the road network pattern characteristics of small and medium cities are not included, and some regions may have insufficient major cities to cover different ages, locations, and development stages. These factors have the potential to lead to underrepresentation of regional patterns. To obtain more comprehensive results, more cities could be involved in the future using our scalable methods. Besides, the demarcation of city boundaries is a ubiquitous question for urban studies (Valencia et al., 2019). In this work, we define an unified study boundary for all cities to facilitate inter-city comparison, and avoid issues arising from varying study boundaries. Although we conduct a preliminary analysis to carefully select the radius based on population, development level, and built-up intensity, the wide difference in urban sizes

inevitably triggers the excessive inclusion of suburbs for some small-size cities, which may introduce biases to the pattern proportions. Besides, more annotated images can be included to improve the robustness and performance of the classification model. While the study produces a massive and fine-grained dataset of road network patterns around the world, covering over 32,000 square kilometer of urban area with a finest resolution of 500 m, we primarily focus on aggregated statistics and analysis to obtain the global landscape, which somewhat wastes the granularity of our dataset. We omit possible fine-grained spatial analysis, such as examining interactions between neighboring road network patterns and exploring relationships between patterns and zoning. Also, the discussion on the influence of topography on road network patterns could be expanded. These research lines could benefit the understanding of urban forms and dynamics. Thus, we invite more targeted or integrated studies on road network patterns on the ground of our open source methods and datasets.

5. Conclusion

Cities are distinguished by their unique urban form, which is largely shaped by road networks. This paper introduces a novel perspective to interpret urban forms using a visual approach natural to humans. The work encompasses 144 major cities globally, considering multiple spatial scales with fine granularity. In our analysis, we are cautious about the scale effect, which are examined and leveraged to obtain multiscale profiles of road network patterns. These profiles demonstrate the continental and dimensional heterogeneity of dominant patterns, highlight inter-city pattern similarities, and uncover characteristics of intra-city pattern spatial distributions. Furthermore, we explore the synergies between road network patterns and socioeconomic and environmental conditions, including GDP, population, and air pollution. Our method and findings can be used to monitor the progress and quality of urban expansion, and assess the impact of the urban form on phenomena such as the urban heat island effect, emissions, and air quality.

Data availability

The spatial data of URNs derives from OpenStreetMap at https://www.openstreetmap.org. The Python package (OSMnx) that we utilize to download OSM data is available at https://github.com/gboeing/. The database of locations and populations of world cities is available at https://simplemaps.com/data/world-cities. The data of WorldPop grids can be accessed at https://www.worldpop.org/. The global nighttime light data is available at https://doi.org/10.7910/DVN/YGIVCD. Country socioeconomic indicators are from the World Bank at https://data.worldbank.org/. The air quality data is from the WHO Air Quality Database at https://www.who.int/data/gho/data/themes/air-pollution/who-air-quality-database . The base map derives from Mapbox at https://www.mapbox.com/maps. The outcome dataset of road network patterns has been uploaded to figshare at https://doi.org/10.6084/m9.figsha or from the corresponding author.

Code availability

All the custom codes related to this paper have been released public at https://github.com/ualsg/Global-road-network-patterns.

Acknowledgements

Author contributions

Additional information

Supplementary Information accompanies this paper at [to be linked at the publication stage].

Competing interests: The authors declare no competing interests.

References

Anselin, L., 1995. Local indicators of spatial association—lisa. Geographical analysis 27, 93–115.

Bafna, S., 2003. Space syntax: A brief introduction to its logic and analytical techniques. Environment and behavior 35, 17–29.

Barrington-Leigh, C., Millard-Ball, A., 2020. Global trends toward urban street-network sprawl. Proceedings of the National Academy of Sciences 117, 1941–1950.

Barthélemy, M., 2011. Spatial networks. Physics Reports 499, 1–101.

Barthelemy, M., 2016. The structure and dynamics of cities. Cambridge University Press.

Bettencourt, L., West, G., 2010. A unified theory of urban living. Nature 467, 912–913.

Biljecki, F., Chow, Y.S., 2022. Global Building Morphology Indicators. Computers, Environment and Urban Systems 95, 101809. doi:10.1016/j.compenvurbsys.2022.101809.

Boeing, G., 2017. Osmnx: New methods for acquiring, constructing, analyzing, and visualizing complex street networks. Computers, Environment and Urban Systems 65, 126–139.

Boeing, G., 2020. A multi-scale analysis of 27,000 urban street networks: Every us city, town, urbanized area, and zillow neighborhood. Environment and Planning B: Urban Analytics and City Science 47, 590–608.

Boeing, G., 2022. Street network models and indicators for every urban area in the world. Geographical Analysis 54, 519–535.

Burghardt, K., Uhl, J.H., Lerman, K., Leyk, S., 2022. Road network evolution in the urban and rural united states since 1900. Computers, Environment and Urban Systems 95, 101803.

Burke, M., Driscoll, A., Lobell, D.B., Ermon, S., 2021. Using satellite imagery to understand and promote sustainable development. Science 371, eabe8628.

Cardillo, A., Scellato, S., Latora, V., Porta, S., 2006. Structural properties of planar graphs of urban street patterns. Physical Review E 73, 066107.

Chen, W., Wu, A.N., Biljecki, F., 2021. Classification of urban morphology with deep learning: Application on urban vitality. Computers, Environment and Urban Systems 90, 101706. URL: https://doi.org/10.1016/j.compenvurbsys.2021.101706, doi:10.1016/j.compenvurbsys.2021.101706.

Chen, Z., Yu, B., Yang, C., Zhou, Y., Yao, S., Qian, X., Wang, C., Wu, B., Wu, J., 2020. An extended time-series (2000-2018) of global NPP-VIIRS-like nighttime light data. URL: https://doi.org/10.7910/DVN/YGIVCD, doi:10.7910/DVN/YGIVCD.

Crucitti, P., Latora, V., Porta, S., 2006. Centrality measures in spatial networks of urban streets. Physical Review E 73, 036125.

Debray, H., Kraff, N.J., Zhu, X.X., Taubenböck, H., 2023. Planned, unplanned, or in-between? a concept of the intensity of plannedness and its empirical relation to the built urban landscape across the globe. Landscape and Urban Planning 233, 104711.

Deng, X., Chen, W., Zhou, Q., Zheng, Y., Li, H., Liao, S., Biljecki, F., 2023. Exploring spatiotemporal pattern and agglomeration of road co2 emissions in guangdong, china. Science of The Total Environment 871, 162134.

Dong, L., Ratti, C., Zheng, S., 2019. Predicting neighborhoods' socioeconomic attributes using restaurant data. Proceedings of the national academy of sciences 116, 15447–15452.

Duren, R.M., Miller, C.E., 2012. Measuring the carbon emissions of megacities. Nature Climate Change 2, 560–562.

Elmqvist, T., Andersson, E., Frantzeskaki, N., McPhearson, T., Olsson, P., Gaffney, O., Takeuchi, K., Folke, C., 2019. Sustainability and resilience for transformation in the urban century. Nature sustainability 2, 267–273.

Elmqvist, T., Fragkias, M., Goodness, J., Güneralp, B., Marcotullio, P.J., McDonald, R.I., Parnell, S., Schewenius, M., Sendstad, M., Seto, K.C., et al., 2013. Urbanization, biodiversity and ecosystem services: challenges and opportunities: a global assessment. Springer Nature.

Frank, L., Bradley, M., Kavage, S., Chapman, J., Lawton, T.K., 2008. Urban form, travel time, and cost relationships with tour complexity and mode choice. Transportation 35, 37–54.

Ganin, A.A., Kitsak, M., Marchese, D., Keisler, J.M., Seager, T., Linkov, I., 2017. Resilience and efficiency in transportation networks. Science advances 3, e1701079.

Gebru, T., Krause, J., Wang, Y., Chen, D., Deng, J., Aiden, E.L., Fei-Fei, L., 2017. Using deep learning and google street view to estimate the demographic makeup of neighborhoods across the united states. Proceedings of the National Academy of Sciences 114, 13108–13113.

Han, B., Sun, D., Yu, X., Song, W., Ding, L., 2020. Classification of urban street networks based on tree-like network features. Sustainability 12, 628.

He, B.J., Ding, L., Prasad, D., 2020. Relationships among local-scale urban morphology, urban ventilation, urban heat island and outdoor thermal comfort under sea breeze influence. Sustainable Cities and Society 60, 102289.

He, K., Zhang, X., Ren, S., Sun, J., 2015. Deep residual learning for image recognition. arXiv:1512.03385.

He, K., Zhang, X., Ren, S., Sun, J., 2016. Identity mappings in deep residual networks. arXiv:1603.05027.

He, Y., Ai, T., Yu, W., Zhang, X., 2017. A linear tessellation model to identify spatial pattern in urban street networks. International Journal of Geographical Information Science 31, 1541–1561.

Heinzle, F., Anders, K., Sester, M., 2007. Automatic detection of pattern in road networks-methods and evaluation, in: Proc. of Joint Workshop Visualization and Exploration of Geospatial Data, Stuttgart, p. 4.

Huang, Y., Lee, C.K., Yam, Y.S., Mok, W.C., Zhou, J.L., Zhuang, Y., Surawski, N.C., Organ, B., Chan, E.F., 2022. Rapid detection of high-emitting vehicles by on-road remote sensing technology improves urban air quality. Science Advances 8, eabl7575.

Ito, K., Biljecki, F., 2021. Assessing bikeability with street view imagery and computer vision. Transportation research part C: emerging technologies 132, 103371.

Jiang, B., Yin, J., Zhao, S., 2009. Characterizing the human mobility pattern in a large street network. Physical Review E 80, 021136.

Kalapala, V., Sanwalani, V., Clauset, A., Moore, C., 2006. Scale invariance in road networks. Physical Review E 73, 026130.

King, A.D., 2012. Colonial urban development: Culture, social power and environment. Routledge.

Kirkley, A., Barbosa, H., Barthelemy, M., Ghoshal, G., 2018. From the betweenness centrality in street networks to structural invariants in random planar graphs. Nature communications 9, 1–12.

Lämmer, S., Gehlsen, B., Helbing, D., 2006. Scaling laws in the spatial structure of urban road networks. Physica A: Statistical Mechanics and its Applications 363, 89–95.

Lemoine-Rodríguez, R., Inostroza, L., Zepp, H., 2020. The global homogenization of urban form. An assessment of 194 cities across time. Landscape and Urban Planning 204, 103949. doi:10.1016/j.landurbplan.2020.103949.

Li, M., Verburg, P.H., Vliet, J.v., 2022. Global trends and local variations in land take per person. Landscape and Urban Planning 218, 104308. doi:10.1016/j.landurbplan.2021.104308.

Li, Y., Yabuki, N., Fukuda, T., 2023. Integrating gis, deep learning, and environmental sensors for multicriteria evaluation of urban street walkability. Landscape and Urban Planning 230, 104603.

Louf, R., Barthelemy, M., 2014. A typology of street patterns. Journal of The Royal Society Interface 11, 20140924.

Ma, L.J., 2002. Urban transformation in china, 1949–2000: a review and research agenda. Environment and planning A 34, 1545–1569.

Maki, F., 1964. Investigations in collective form. The School of Architecture .

Marshall, S., 2004. Streets and patterns. Routledge.

Marshall, S., Gil, J., Kropf, K., Tomko, M., Figueiredo, L., 2018. Street network studies: from networks to models and their representations. Networks and Spatial Economics 18, 735–749.

Marshall, W.E., Garrick, N.W., 2010. Effect of street network design on walking and biking. Transportation Research Record 2198, 103–115.

Marshall, W.E., Garrick, N.W., 2011. Does street network design affect traffic safety? Accident Analysis & Prevention 43, 769–781.

Masucci, A.P., Smith, D., Crooks, A., Batty, M., 2009. Random planar graphs and the london street network. The European Physical Journal B 71, 259–271.

Middel, A., Lukasczyk, J., Zakrzewski, S., Arnold, M., Maciejewski, R., 2019. Urban form and composition of

street canyons: A human-centric big data and deep learning approach. Landscape and Urban Planning 183, 122–132.

Moran, P.A., 1950. Notes on continuous stochastic phenomena. Biometrika 37, 17–23.

Moudon, A.V., 1997. Urban morphology as an emerging interdisciplinary field. Urban morphology 1, 3–10.

Openshaw, S., 1981. The modifiable areal unit problem. Quantitative geography: A British view , 60–69.

OpenStreetMap contributors, 2017. Planet dump retrieved from https://planet.osm.org . https://www.openstreetmap.org.

Ortman, S.G., Cabaniss, A.H., Sturm, J.O., Bettencourt, L.M., 2014. The pre-history of urban scaling. PloS one 9, e87902.

Pasha, M., Rifaat, S.M., Tay, R., De Barros, A., 2016. Effects of street pattern, traffic, road infrastructure, socioeconomic and demographic characteristics on public transit ridership. KSCE Journal of Civil Engineering 20, 1017–1022.

Patias, N., Rowe, F., Cavazzi, S., Arribas-Bel, D., 2021. Sustainable urban development indicators in Great Britain from 2001 to 2016. Landscape and Urban Planning 214, 104148. doi:10.1016/j.landurbplan.2021.104148.

Porta, S., Crucitti, P., Latora, V., 2006. The network analysis of urban streets: a primal approach. Environment and Planning B: planning and design 33, 705–725.

Rifaat, S.M., Tay, R., de Barros, A., 2012. Urban street pattern and pedestrian traffic safety. Journal of urban design 17, 337–352.

Rifaat, S.M., Tay, R., De Barros, A., 2011. Effect of street pattern on the severity of crashes involving vulnerable road users. Accident Analysis & Prevention 43, 276–283.

Shannon, C.E., 1948. A mathematical theory of communication. The Bell system technical journal 27, 379–423.

Snellen, D., Borgers, A., Timmermans, H., 2002. Urban form, road network type, and mode choice for frequently conducted activities: A multilevel analysis using quasi-experimental design data. Environment and Planning A: Economy and Space 34, 1207–1220. URL: https://doi.org/10.1068/a349, doi:10.1068/a349.

Southworth, M., Ben-Joseph, E., 2013. Streets and the Shaping of Towns and Cities. Island Press.

SteadieSeifi, M., Dellaert, N.P., Nuijten, W., Van Woensel, T., Raoufi, R., 2014. Multimodal freight transportation planning: A literature review. European journal of operational research 233, 1–15.

Strano, E., Viana, M., da Fontoura Costa, L., Cardillo, A., Porta, S., Latora, V., 2013. Urban street networks, a comparative analysis of ten european cities. Environment and Planning B: Planning and Design 40, 1071–1086.

Sun, L., Chen, J., Li, Q., Huang, D., 2020. Dramatic uneven urbanization of large cities throughout the world in recent decades. Nature communications 11, 1–9.

Szegedy, C., Liu, W., Jia, Y., Sermanet, P., Reed, S., Anguelov, D., Erhan, D., Vanhoucke, V., Rabinovich, A., 2015. Going deeper with convolutions, in: Proceedings of the IEEE conference on computer vision and pattern recognition, pp. 1–9.

Tian, J., Song, Z., Gao, F., Zhao, F., 2016. Grid pattern recognition in road networks using the c4. 5 algorithm. Cartography and Geographic Information Science 43, 266–282.

Tian, Y., Tsendbazar, N.E., Leeuwen, E.v., Fensholt, R., Herold, M., 2022. A global analysis of multifaceted urbanization patterns using Earth Observation data from 1975 to 2015. Landscape and Urban Planning 219, 104316. doi:10.1016/j.landurbplan.2021.104316.

Valencia, S.C., Simon, D., Croese, S., Nordqvist, J., Oloko, M., Sharma, T., Taylor Buck, N., Versace, I., 2019. Adapting the sustainable development goals and the new urban agenda to the city level: Initial reflections from a comparative research project. International Journal of Urban Sustainable Development 11, 4–23.

Van Houtan, K.S., Tanaka, K.R., Gagné, T.O., Becker, S.L., 2021. The geographic disparity of historical greenhouse emissions and projected climate change. Science Advances 7, eabe4342.

Wang, J., Fleischmann, M., Venerandi, A., Romice, O., Kuffer, M., Porta, S., 2023. Eo+ morphometrics: Understanding cities through urban morphology at large scale. Landscape and Urban Planning 233, 104691.

Wang, X., You, S., Wang, L., 2017. Classifying road network patterns using multinomial logit model. Journal of Transport Geography 58, 104–112.

Whittemore, A.H., 2012. Zoning los angeles: a brief history of four regimes. Planning Perspectives 27, 393–415.

WorldPop, 2018. Global 1km population. doi:10.5258/SOTON/WP00647.

Wu, A.N., Biljecki, F., 2022. Ganmapper: geographical data translation. International Journal of Geographical Information Science 36, 1394–1422.

Wu, A.N., Biljecki, F., 2023. InstantCITY: Synthesising morphologically accurate geospatial data for urban form analysis, transfer, and quality control. ISPRS Journal of Photogrammetry and Remote Sensing 195, 90–104.

Wu, C.Y., Hu, M.B., Jiang, R., Hao, Q.Y., 2021. Effects of road network structure on the performance of urban traffic systems. Physica A: Statistical Mechanics and its Applications 563, 125361.

Wu, F., Xu, J., Yeh, A.G.O., 2006. Urban development in post-reform China: state, market, and space. Routledge.

Xie, F., Levinson, D., 2007. Measuring the structure of road networks. Geographical analysis 39, 336–356.

Xu, Y., Olmos, L.E., Abbar, S., González, M.C., 2020. Deconstructing laws of accessibility and facility distribution

in cities. Science advances 6, eabb4112.

Xu, Y., Ren, C., Ma, P., Ho, J., Wang, W., Lau, K.K.L., Lin, H., Ng, E., 2017. Urban morphology detection and computation for urban climate research. Landscape and Urban Planning 167, 212–224. doi:10.1016/j.landurbplan.2017.06.018.

Xue, J., Jiang, N., Liang, S., Pang, Q., Yabe, T., Ukkusuri, S.V., Ma, J., 2022. Quantifying the spatial homogeneity of urban road networks via graph neural networks. Nature Machine Intelligence 4, 246–257.

Yang, B., Luan, X., Li, Q., 2010. An adaptive method for identifying the spatial patterns in road networks. Computers, Environment and Urban Systems 34, 40–48.

Zhu, X.X., Qiu, C., Hu, J., Shi, Y., Wang, Y., Schmitt, M., Taubenböck, H., 2022. The urban morphology on our planet–global perspectives from space. Remote Sensing of Environment 269, 112794.

Supplementary Information

Global Urban Road Network Patterns: Unveiling multiscale planning paradigms of 144 cities with a novel deep learning approach

Wangyang Chen[1,2,3]**, Huiming Huang**[1,2,3]**, Shunyi Liao**[1,2,3]**, Feng Gao**[1,2,3]**, Filip Biljecki**[4,5,*]

[1] *Guangzhou Urban Planning & Design Survey Research Institute, Guangzhou, 510060, China*

[2] *Collaborative Innovation Center for Natural Resources Planning and Marine Technology of Guangzhou, Guangzhou, 510060, China*

[2] *Guangdong Enterprise Key Laboratory for Urban Sensing, Monitoring and Early Warning, Guangzhou, 510060, China*

[4] *Department of Architecture, National University of Singapore, Singapore*

[5] *Department of Real Estate, National University of Singapore, Singapore*

[*] *Corresponding Author*

Supplementary Notes

Supplementary Figures

Supplementary Tables

1 Supplementary Note 1: Colored Road Hierarchical Diagram (CRHD)

1.1 Definition of CRHD

Colored Road Hierarchical Diagram (CRHD) is a type of diagram that maps different grades of roads with varying widths and colors in a cartographic manner[1]. Its merits include enhanced legibility for machines and convenience for preprocessing. Since the seminal paper does not expound on the details about the feature and generation of CRHD, we provide additional elaborations here.

After retrieving the spatial data of roads in a specified scope (receptive field), the CRHD is created using *CRHD generator*, which is upgraded from the open-source Python tool provided by ref.[1]. Roads are sequentially plotted with different widths and colors using the road class attribute (`fclass`) in OpenStreetMap (OSM). The original road classes are condensed into five groups, including motorway, primary road, secondary road, tertiary road and service road. Since we use white as the background color of a CRHD, we assign darker colors to higher-class roads with a colormap from skyblue to black. Exceptionally, we mark motorways using a distinct color (darkred) to outline its special position, given the fact that motorway is considered to have different nature from the other roads during network modeling[2,3]. Although the selection of colors for each road grade are rigorously testified, in our experiment, we find that the model trained on CRHDs achieves a significantly higher overall accuracy (0.92) than that trained on monochrome diagrams (0.70). Another study suggests improved performance by using different color combination[4]. It implies that coloring matters more than the selection of colors.

1.2 Outreach of CRHD

A CRHD could be considered as a snapshot of urban road networks (URNs) within a designated boundary. We regard the scope of the CRHD as the receptive field acting on the complete URNs, and based on that, the pattern of the covered subnetwork is classified. Since URN is a sort of continuum, other than the scale effect discussed in the main text, it is also inevitable to consider the interactions among the neighborhoods when exerting pattern classification on separate urban grids. To consider that, when generating the CRHD for a grid, we define 'outreaches' that expand the receptive field beyond the grid. In this study, the existence of outreaches also facilitates the CRHD operations (see the next subsection — Section 1.3). The width of the outreach is defined empirically. We posit that the neighboring effect would be more significant at smaller scale. Microscopically, the concerned roads tend to be a component of a larger network, and in this case, the interplay and cooperation between ambient roads is more negligible. Therefore, we assign relatively wider outreaches for the small-scale and mid-scale grids (a half of the grid width) than large-scale grids (a quarter of the grid width) (Fig. 1a). From another perspective, CRHDs with outreaches are similar with that of convolution kernels in the field of computer vision (Fig. 1b). It lays the foundation for deeply understanding the urban form of the whole city.

1.3 CRHD operations

To conduct multiscale analysis based on CRHDs collected at single scale, tools to rescale CRHDs is necessary. Stitching operation is used to upscale the CRHDs. It merges four neighboring CRHDs into a larger one (Fig. 1c). Correspondingly, for downscaling, we have the subsampling operation, which extracts smaller-scale CRHDs from the source CRHD (Fig. 1d). Other than the merit of abbreviated data collection, considering the internet-dependent and time-consuming process of CRHD generation, the operations also accelerate the process of multiscale pattern classification. The Python codes for the operations would be released open source.

1.4 Pattern classification

Our road network pattern classification model applies the ResNets architecture[5,6]. In our experiments, we find that ResNet-34 outperforms the other members in the ResNets family in our tasks. Thus, we choose this specific architecture (Supplementary Fig. 1e) to establish our model. As an important branch of convolutional neural networks (CNN), ResNets is notable for the design of 'shortcuts', and achieves favorable performances in various tasks. The model architecture is stacked by a series of standardized residual blocks. A residual block is defined as:

$$y = F(x, \{W_i\}) + W_s x \tag{1}$$

where x and y are the input and output vectors, respectively. Function $F(x, \{W_i\})$ is the residual mapping to be learned. The addition of an extra x in the end serves as a shortcut connection. W_s is only used when matching dimensions.

Based on the mid-scale CRHD set and above-mentioned CRHD operations, we are able to obtain all small-scale, mid-scale and large-scale CRHDs in our cities of interest. CRHDs at all the scales are resized into 224×224 and fed into the pattern classification model. The model returns a 6×1 vector indicating the predictive probabilities of being each pattern category. The category with the highest probability would be regarded as the final pattern.

a

Receptive field
1000m
Outreach
500m
250m
grid
Small

2000m
1000m
500m
Mid

5000m
2000m
500m
Large

b

Feature map
Pixel
Kernel
Receptive field
Image
Image and convolution kernel

Pattern map
Grid cell
CRHD
Receptive field
Meshed city
Outreach
City and CRHD

c

Top left
Top right
Stitching
Bottom left
Bottom right
Mid-scale CRHDs in a group

Large-scale CRHD

d

Mid-scale CRHD

Top left
Top right
Subsampling
Bottom left
Bottom right
Small-scale CRHDs

e

output size: 112×112　output size: 56×56　output size: 28×28　output size: 14×14　output size: 7×7　output size: 49×1　output size: 6×1

CRHD → 7x7 conv, 64, /2 → pool, /2 → [×3] 3x3 conv, 64 / 3x3 conv, 64 → [×1] 3x3 conv, 128, /2 / 3x3 conv, 128 → [×3] 3x3 conv, 128 / 3x3 conv, 128 → [×1] 3x3 conv, 256, /2 / 3x3 conv, 256 → [×5] 3x3 conv, 256 / 3x3 conv, 256 → [×1] 3x3 conv, 512, /2 / 3x3 conv, 512 → [×2] 3x3 conv, 512 / 3x3 conv, 512 → avg pool, flatten → full-connected 3 → Probabilities/ category

Supplementary Figure 1. Introduction of CRHDs, CRHD operations, and the architecture of the classification model. a The sizes of grids and corresponding CRHDs at small, mid, and large scales. The green squares in the middle are the urban grid and the yellow bounds represent the associated outreaches. Together, they constitute the receptive field of a CRHD. **b** The analogy between a convolution kernel and a CRHD. The process of classifying URN patterns by CRHDs is similar with conducting convolutions on images. The diagram shows the matchup of concepts between the two. **c** Stitching operation. It merges the CRHDs of four neighboring grids into a larger-scale one. The process is achieved by truncating the repetitive areas (edge areas) of the input diagrams and concatenating them based on pixel-level matching on the edges. After that, the width of outreaches remains the same. **d** Subsampling operation. It splits a CRHD into four smaller-scale ones that contain the road information of grids with outreaches in each corner. The operation is realized by slicing the CRHD by bounding boxes with varying positions. **e** The architecture of our pattern classification model (ResNet-34).

2 Supplementary Note 2: Training process and model performance
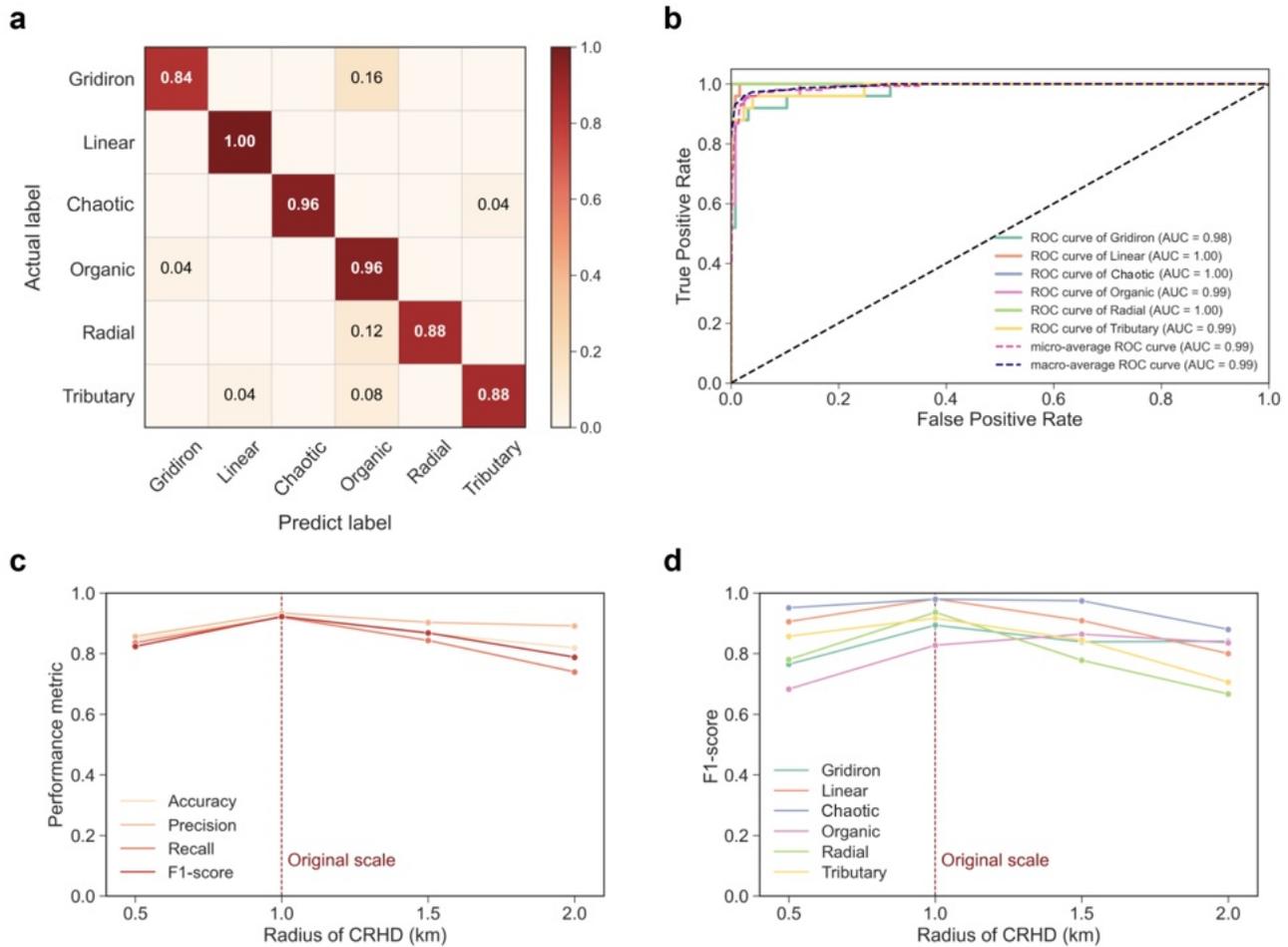
Supplementary Figure 2. Performance of the pattern classification model. a The confusion matrix evaluated by test set at original scale. The numbers on the diagonal denote the accuracy for each pattern. The numbers elsewhere refer to the rates of misclassifying the category in the row into the one in the column. **b** ROC curves and the corresponding AUC values of micro-average, macro-average and each category at original scale. **c** Variation of performance metrics (overall accuracy, precision, recall and f1-score) of the model at different scales. **d** Variation of f1-scores of individual categories at different scales.

2.1 Training process

The model is trained on a manually annotated image set including 1,548 CRHDs at mid scale. CRHDs selected into the image set must be easily discernible and present minimum pattern mixture. The image set is split randomly into training (80%), validation (10%) and test (10%) sets. Since we would apply the model in numerous cities worldwide, the samples are selected dispersively from different cities and continents. Given a dataset with relatively small size, we adopt data augmentation (random flip, rotation and scale) during the training process to enrich the dataset and enhance the robustness of the model. Our best performance model is trained with a batch size of 16, a learning rate of 0.00005, and a maximum epoch of 50.

2.2 Evaluation of cross-scale performance

We regard road network pattern as a domestic feature, which means the scale must be definite when the pattern is perceived. The pattern may vary significantly at the same position due to scale effect. As the model is trained with CRHDs at invariable scale, its applicability at other scales should be examined. For this purpose, we replicate the centroids of the CRHDs in the test set, and generate CRHDs with fluctuating radius to establish test sets at different scales. Because some patterns would alter in this process, we inspect and update the annotations of these derivative test sets. The performance of the model at multiple scales are then evaluated. As it is shown in Fig. 2c, the model works best at the original scale as expected. All the metrics

drop when the scale deviates from the initial scale. More details behind the performance decay could be found in Fig. 2d. At a smaller scale, there is a clear decline in the f1-score of organic. A possible explanation is that organic is primarily formed by circuits of major roads in the training set. A shrinking scale excludes part of the major roads, leaving the model an unfamiliar situation where major and secondary roads constitute circuits together. The assumption is supported by the better performance for organic at larger scale. Conversely, f1-scores for radial and tributary get worse during upscaling. Radial and tributary are characterized by radiated or unclosed major roads. When the receptive field is enlarged, more roads are involved, which encourages the presence of road major road circuits and thus leads to misclassifications. To conclude, although performance decay exists because of scale variation, the overall f1-score only reduces by 14.5% from the best (1000 m) to the worst (2000 m) occasion, which we believe acceptable in this study.

3 Supplementary Note 3: Study boundary radius selection

The size of urban centers varies greatly across different cities. A proper definition of study boundary for the cities is the premise of conducting further analysis. One option is to use morphological boundaries derived from satellite remote-sensing data (such as Global Human Settlement Layer (GHSL) Data Package). GHSL provides a layer of the degree of urbanization, which distinguishes the urban center (high density cluster) and suburban areas worldwide. However, different scales in urban centers among the cities bring difficulties to the road network pattern analysis. For cities with large urban centers, including a large study area may dilute a city's unique road network pattern characteristics, which are usually reflected in the core urban area. Among our cities of interest, large cities (e.g. London, Paris, etc.) may possess a urban center scale over ten times as that of the small cities (e.g. Sevilla, Odesa, etc.). We cannot rule out the influence of scale differences between cities when comparing their overall road network patterns. Meanwhile, although our data acquisition is mostly automated, collecting CRHDs is still pretty time-consuming due to the online inquiry process with OSMnx.

Thus, to avoid the issues above, we decide to use a consistent study boundary (a buffer from the city center) for all the cities. To determine a proper buffer radius, we introduce three auxiliary indicators from the perspective of population, development level, and built-up intensity, respectively. First, using the total population data from SimpleMaps and the gridded population data from WorldPop (2020), we calculate the average proportion of population covered by buffer zones with radii ranging from 5 km to 40 km in the cities. Second, we harness nighttime light data (NTL) to reflect the general urban development level. With the annual NPP-VIIRS-like NTL data (2020)[7], we obtain the average NTL brightness for each radius, and normalize the value to 0-100 by dividing the maximum. The average normalized NTL brightness in the cities is the second indicator. Last, the proportion of urban center area within the buffer is used to measure the built-up intensity of each radius. The variation of the indicators over different radii is illustrated in Supplementary Fig. 3a. Generally, we prefer a radius that can achieve more population coverage, higher NTL brightness, and stronger built-up intensity. We end up with a radius of 15 km, which yields moderate values for all the indicators, as a joint consideration from the three aspects. On average, this radius covers 57.8% of the total population, with an average NTL brightness of 70.1% of the brightest zone and 72.7% of the area covered by the city center.

To further examine the selection, we demonstrate the extreme cases obtained with the 15 km radius for each indicators (Supplementary Fig. 3b). A 15 km-buffer may cover more people than the total population of some cities (e.g. Medellin, Colombia). It is mainly due to the heavy population concentration and the underestimated total population. The covered population could also be minor for the cities with only a small part of the population in the main city and most of the population scattered in subordinate counties (e.g. Nanyang, China). Similar situation could also occur for the cities with small urban centers (e.g. Ganzhou, China). The normalized NTL brightness for 15 km radius is influenced by the relative location between the geographical and functional city centers. When both centers are misaligned by some distance, the brightness tends to be high. When both centers overlap in space and the city scale is small, the 5 km-radius area tends to be the brightest and the brightness for 15 km radius becomes lower. For the cases mentioned so far, the main urban area is well included by the study boundary. For megacities such as Paris, although the 15 km buffer cannot cover the whole urban center areas, it involves the most historic and distinctive areas. In summary, defining consistent study boundaries as a 15 km-radius buffer is well suited to the needs of the research.
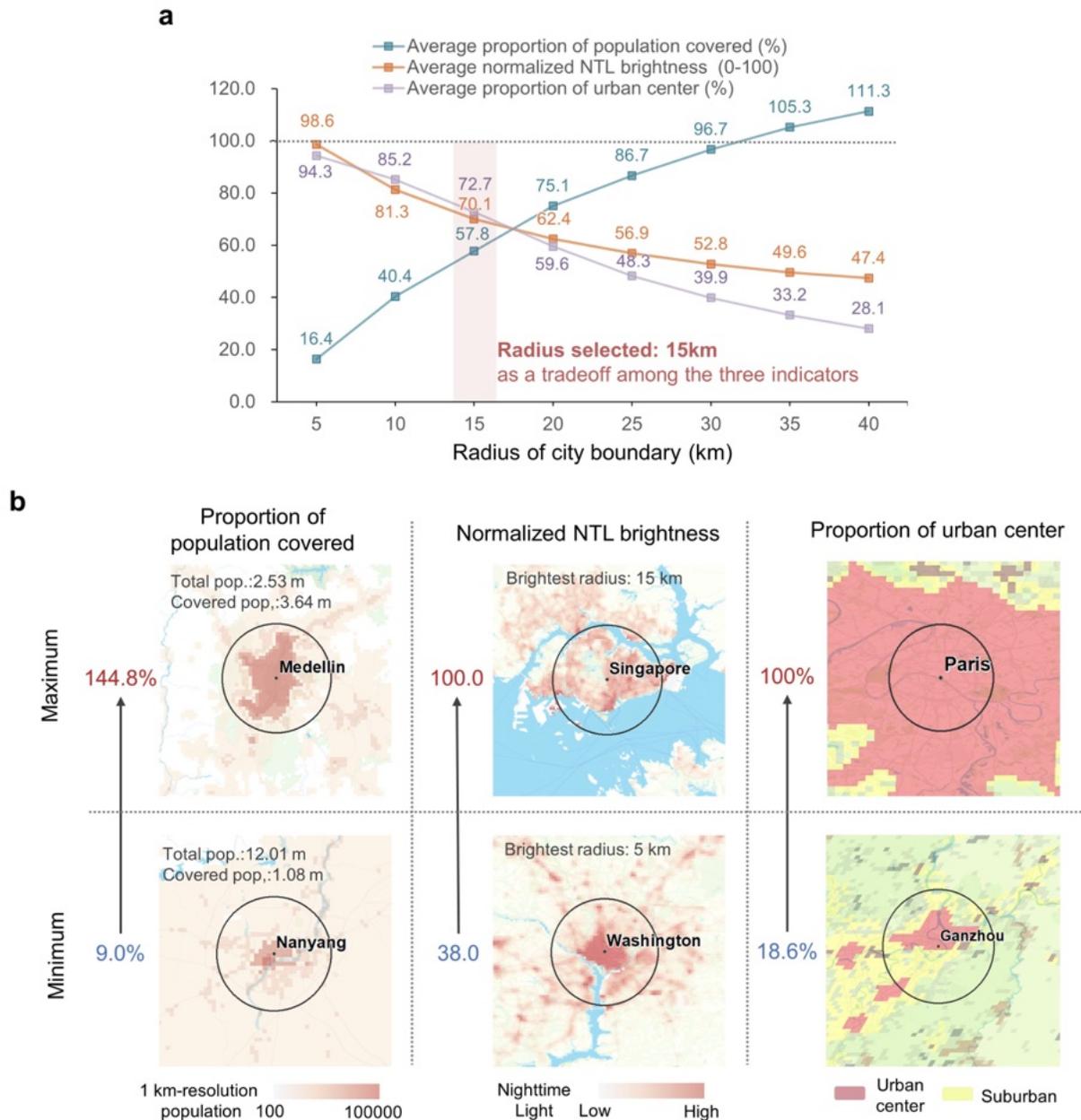
Supplementary Figure 3. Process and validation of the study boundary radius selection. a Variation of indicators with different study boundary radii. The abscissa indicates different radius from 5 km to 40 km, while the ordinate denotes the values of three indicators: (1) average proportion of population covered (%), (2) average normalized NTL brightness (0-100), and (3) average proportion of urban center (%). **b** Example maps of cities with an extreme state of indicators. From left to right is the spatial distribution map of city pairs with the maximum and minimum values of each indicator. The black circle indicates the 15 km-radius study boundary. Source of the base map: (c) Mapbox.
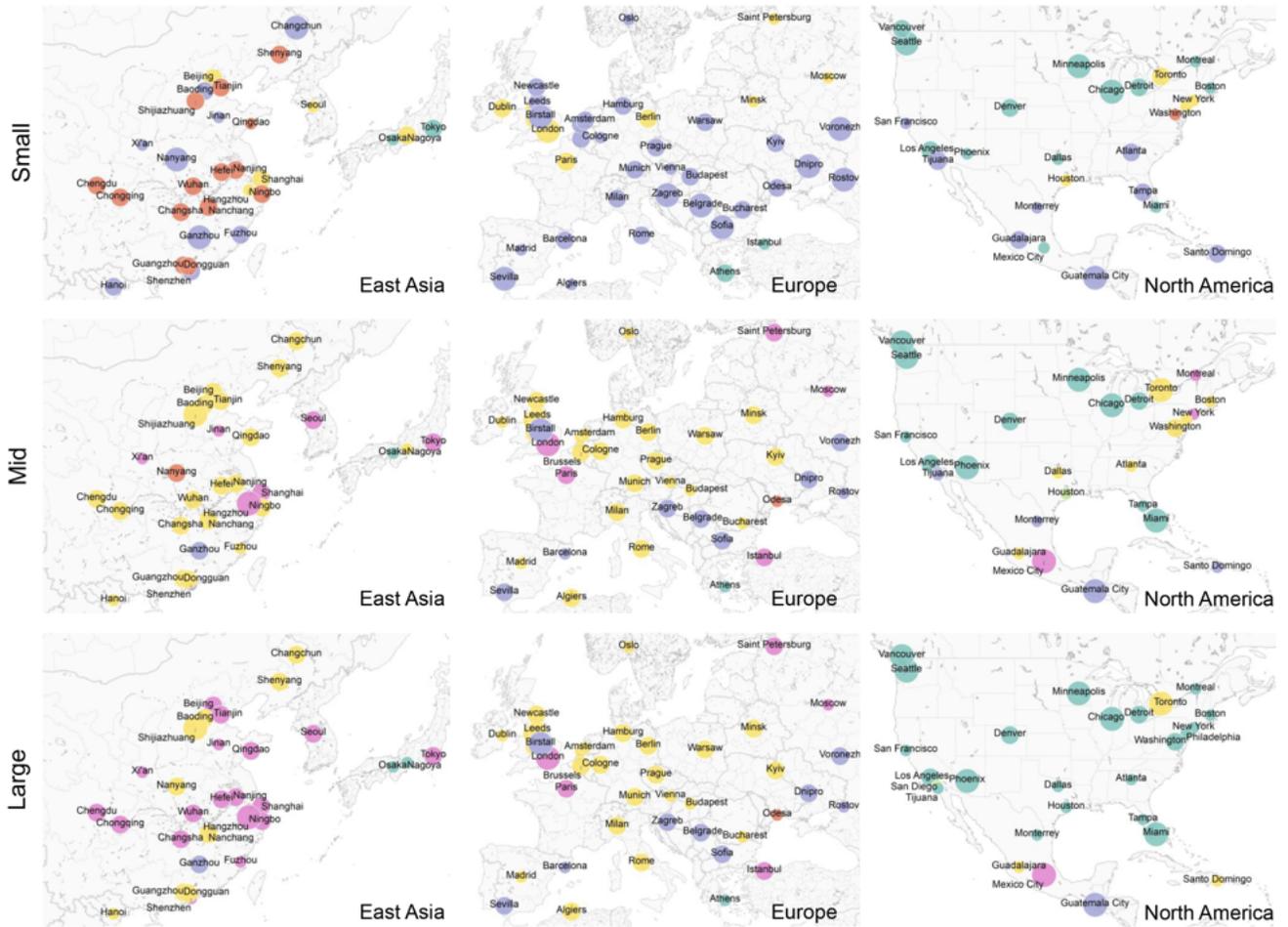
Supplementary Figure 4. Zoomed-in maps of dominant patterns in regions with dense cities of interest. The regions include East Asia, Europe and North America.
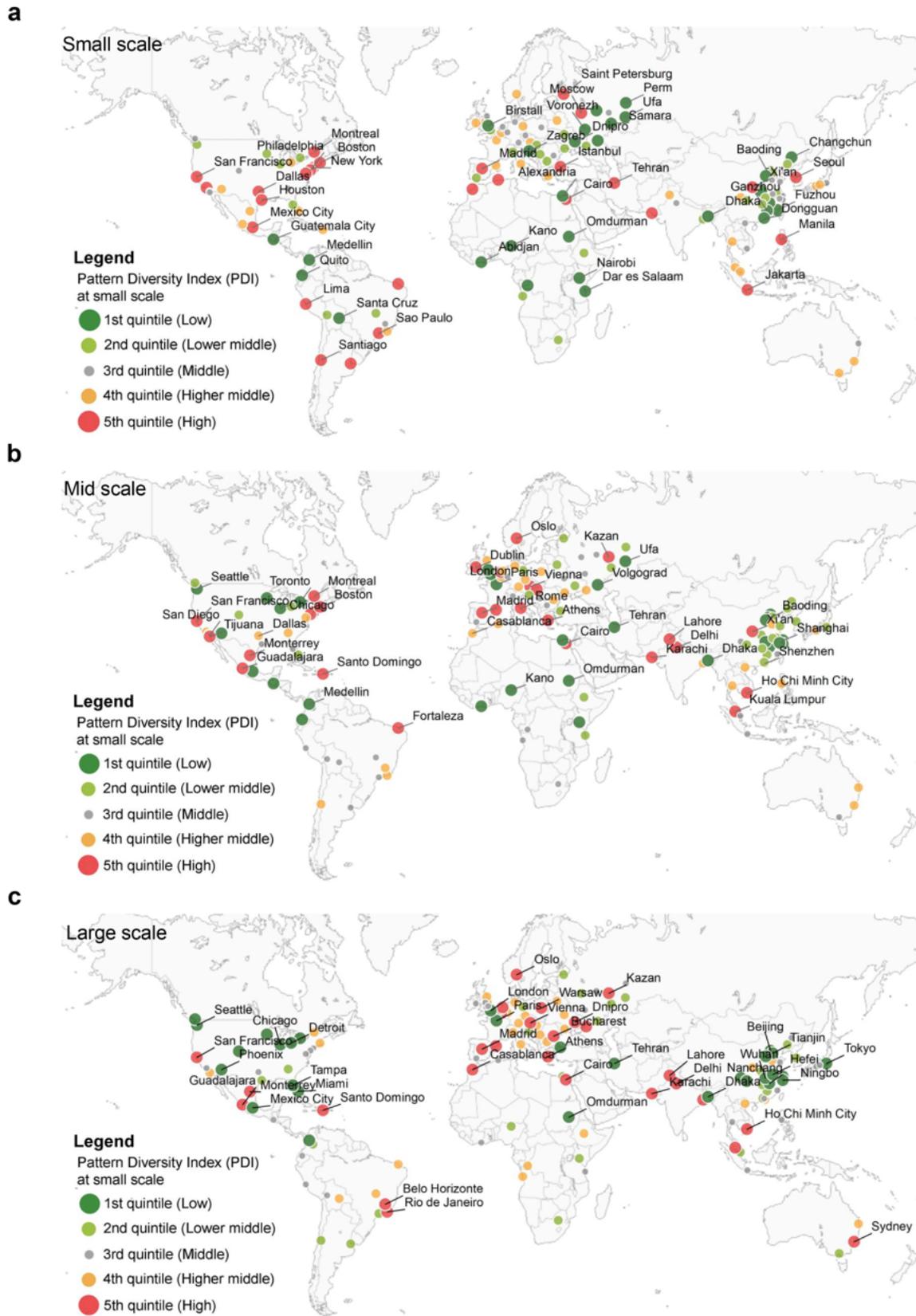
Supplementary Figure 5. Distribution of cities with Pattern Diversity Index (PDI) at different scales: a small, b mid, c large. PDIs are divided into five groups based on quintiles. The point color indicates the degree of deviation from the median PDI. Grey is around the median, green means approaching the lower bound, and red means approaching the upper bound. Cities lying in the 1st and 5th quintiles are labelled with names on the maps. PDI values at all scales for individual cities could be found in Supplementary Table 6.
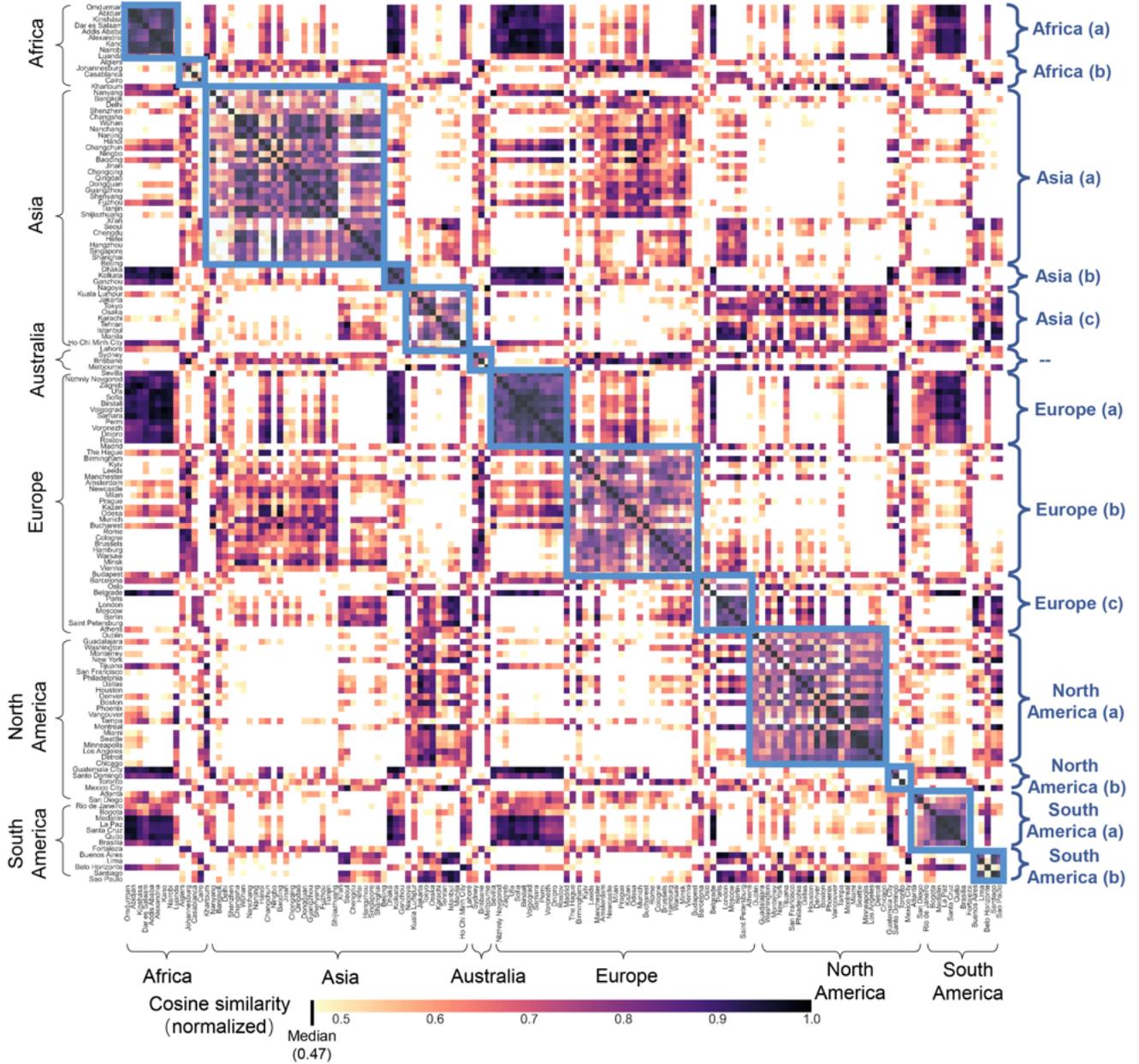
Supplementary Figure 6. Inter-city pattern similarity matrix. After pattern convolution, each city is embedded by the pattern proportions (a 18-dimension feature vector). The cities and their pattern proportions form a 144 × 18 feature matrix. We standardize each column to be normally distributed, calculate the cosine similarity between each pair of cities, and obtain a 144 × 144 similarity matrix. For easier interpretation, the cosine similarity scores are normalized to 0 to 1 by the maximum and minimum. Only the cells with the similarity score above the median (0.47) are visible. To discover the potential subgrouping among the cities, we reorder the similarity matrix in a special way. First, cities from the same continent are aligned together. Then, the cities in each continent are ranked by their average similarities with the cities in the same continent and those outside. Note that all the average similarities are replaced by ranges to loosen the constraint of absolute number size and inject more flexibility for grouping. The number of ranges are set as 4 with the best experimental performance. As we keep the similarity matrix symmetric, every square of dark cells on the diagonal indicates a potential subgroup of cities in the continent. There are totally 13 subgroups, including 2 in Africa, 3 in Asia, 1 in Australia, 3 for Europe, 2 for North America, and 2 for South America. The subgroups are annotated separately for each continent in alphabetical order.
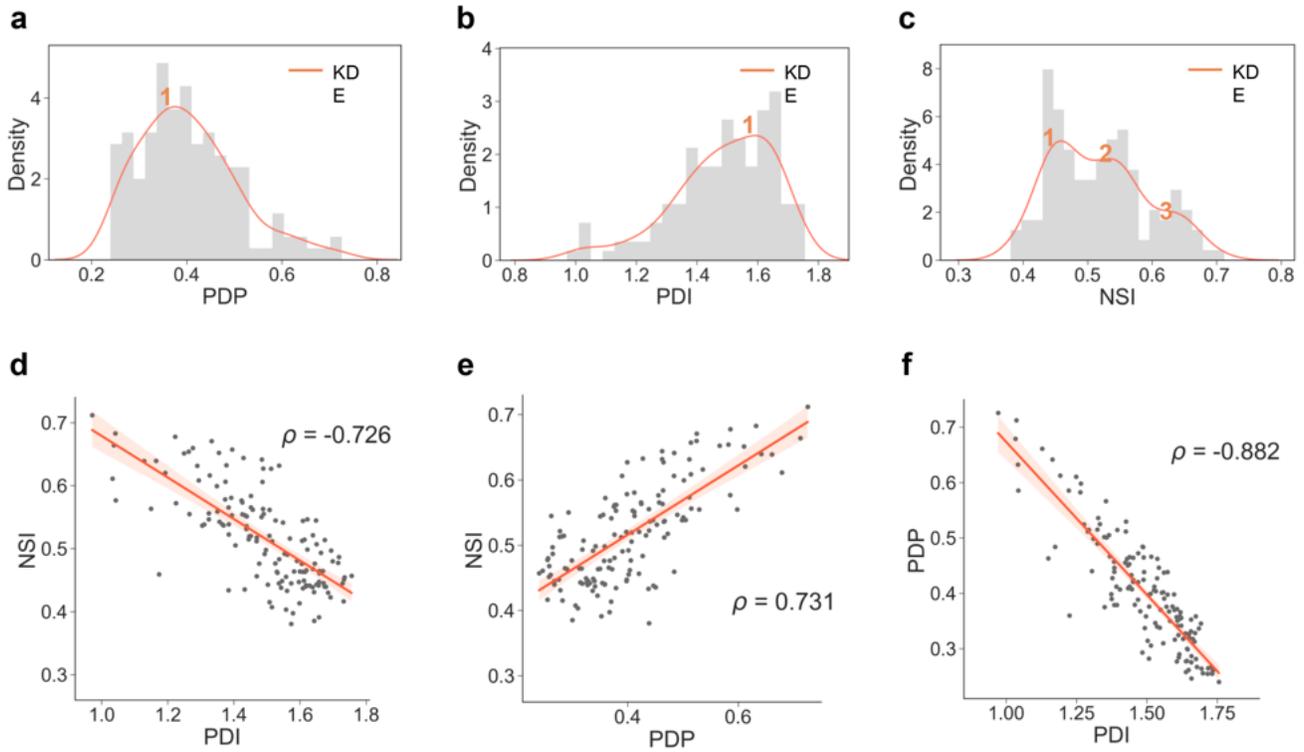
Supplementary Figure 7. Distribution of the pattern indicators and the pairwise correlations among them. a, **b**, and **c** are the histograms and kernel density estimate curves (KDEs), which describe the distribution of PDPs, PDIs and NSIs of cities of interest respectively. The numbers above the curves mark the peaks of the KDEs. **d**, **e** and **f** demonstrate the correlations between each pair of the three indicators, together with the corresponding Pearson correlation coefficient (ρ).
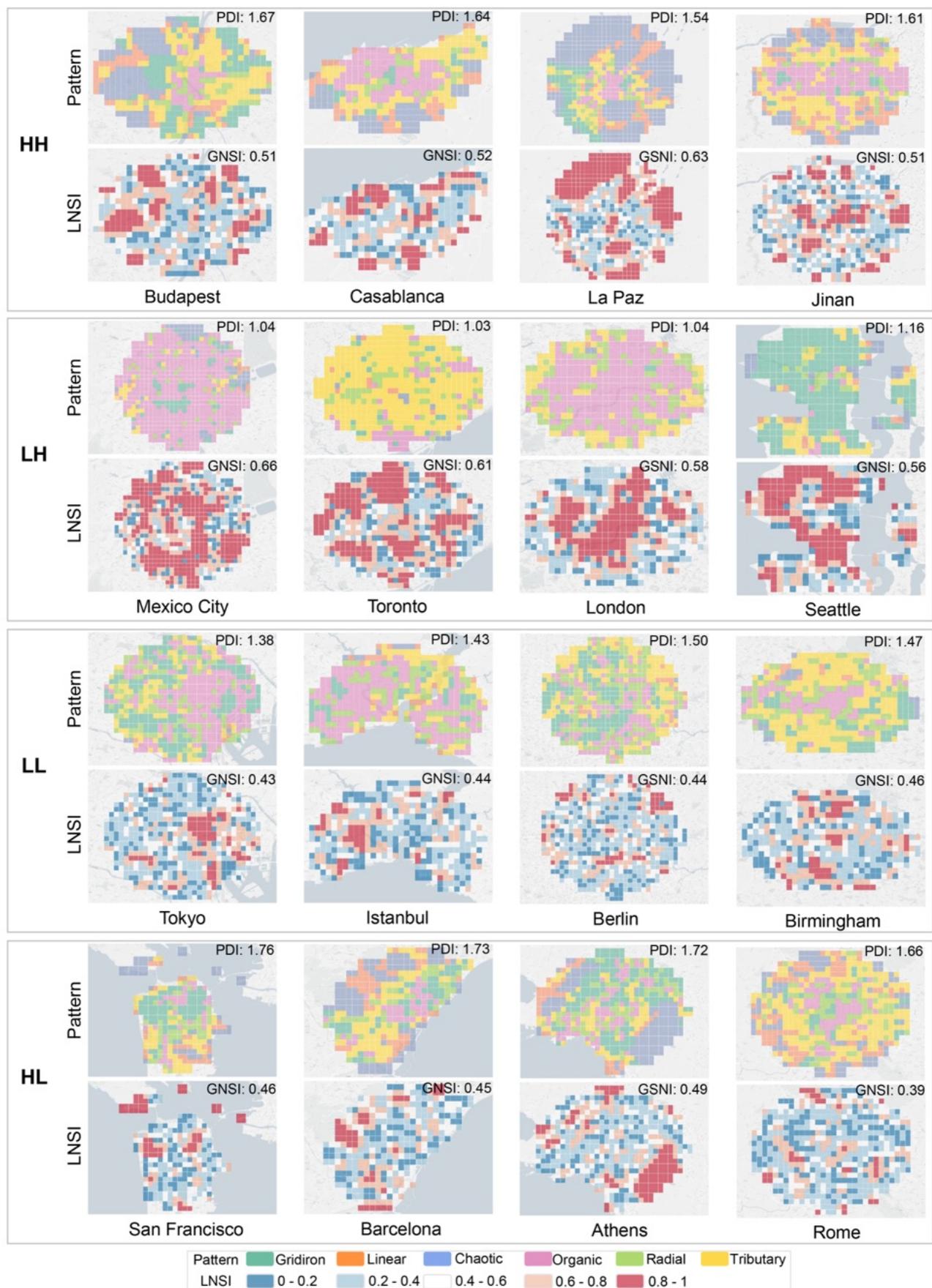
Supplementary Figure 8. Pattern and LNSI maps at mid scale for representative cities in each quadrant. **a** HH, **b** LH, **c** LL and **d** HL groups. The corresponding PDI and GNSI are labelled at top right.

Supplementary Table 1. List of cities of interest (alphabetical order by continent and country).

No.	City	Country	Continent	No.	City	Country	Continent
1	Algiers	Algeria	Africa	73	Budapest	Hungary	Europe
2	Luanda	Angola	Africa	74	Dublin	Ireland	Europe
3	Kinshasa	Congo	Africa	75	Milan	Italy	Europe
4	Abidjan	Cte D'Ivoire	Africa	76	Rome	Italy	Europe
5	Alexandria	Egypt	Africa	77	Amsterdam	Netherlands	Europe
6	Cairo	Egypt	Africa	78	The Hague	Netherlands	Europe
7	Addis Ababa	Ethiopia	Africa	79	Oslo	Norway	Europe
8	Nairobi	Kenya	Africa	80	Warsaw	Poland	Europe
9	Casablanca	Morocco	Africa	81	Bucharest	Romania	Europe
10	Kano	Nigeria	Africa	82	Kazan	Russia	Europe
11	Johannesburg	South Africa	Africa	83	Moscow	Russia	Europe
12	Khartoum	Sudan	Africa	84	Nizhniy Novgorod	Russia	Europe
13	Omdurman	Sudan	Africa	85	Perm	Russia	Europe
14	Dar es Salaam	Tanzania	Africa	86	Rostov	Russia	Europe
15	Dhaka	Bangladesh	Asia	87	Saint Petersburg	Russia	Europe
16	Baoding	China	Asia	88	Samara	Russia	Europe
17	Beijing	China	Asia	89	Ufa	Russia	Europe
18	Changchun	China	Asia	90	Volgograd	Russia	Europe
19	Changsha	China	Asia	91	Voronezh	Russia	Europe
20	Chengdu	China	Asia	92	Belgrade	Serbia	Europe
21	Chongqing	China	Asia	93	Barcelona	Spain	Europe
22	Dongguan	China	Asia	94	Madrid	Spain	Europe
23	Fuzhou	China	Asia	95	Sevilla	Spain	Europe
24	Ganzhou	China	Asia	96	Dnipro	Ukraine	Europe
25	Guangzhou	China	Asia	97	Kyiv	Ukraine	Europe
26	Hangzhou	China	Asia	98	Odesa	Ukraine	Europe
27	Hefei	China	Asia	99	Birmingham	United Kingdom	Europe
28	Jinan	China	Asia	100	Birstall	United Kingdom	Europe
29	Nanchang	China	Asia	101	Leeds	United Kingdom	Europe
30	Nanjing	China	Asia	102	London	United Kingdom	Europe
31	Nanyang	China	Asia	103	Manchester	United Kingdom	Europe
32	Ningbo	China	Asia	104	Newcastle	United Kingdom	Europe
33	Qingdao	China	Asia	105	Montreal	Canada	North America
34	Shanghai	China	Asia	106	Toronto	Canada	North America
35	Shenyang	China	Asia	107	Vancouver	Canada	North America
36	Shenzhen	China	Asia	108	Santo Domingo	Dominican Republic	North America
37	Shijiazhuang	China	Asia	109	Guatemala City	Guatemala	North America
38	Tianjin	China	Asia	110	Guadalajara	Mexico	North America
39	Wuhan	China	Asia	111	Mexico City	Mexico	North America
40	Xi'an	China	Asia	112	Monterrey	Mexico	North America
41	Delhi	India	Asia	113	Tijuana	Mexico	North America
42	Kolkata	India	Asia	114	Atlanta	United States	North America
43	Jakarta	Indonesia	Asia	115	Boston	United States	North America
44	Tehran	Iran	Asia	116	Chicago	United States	North America
45	Nagoya	Japan	Asia	117	Dallas	United States	North America
46	Osaka	Japan	Asia	118	Denver	United States	North America
47	Tokyo	Japan	Asia	119	Detroit	United States	North America
48	Seoul	Korea	Asia	120	Houston	United States	North America
49	Kuala Lumpur	Malaysia	Asia	121	Los Angeles	United States	North America
50	Karachi	Pakistan	Asia	122	Miami	United States	North America
51	Lahore	Pakistan	Asia	123	Minneapolis	United States	North America
52	Manila	Philippines	Asia	124	New York	United States	North America
53	Singapore	Singapore	Asia	125	Philadelphia	United States	North America
54	Bangkok	Thailand	Asia	126	Phoenix	United States	North America
55	Istanbul	Turkey	Asia	127	San Diego	United States	North America
56	Hanoi	Vietnam	Asia	128	San Francisco	United States	North America
57	Ho Chi Minh City	Vietnam	Asia	129	Seattle	United States	North America
58	Brisbane	Australia	Australia	130	Tampa	United States	North America
59	Melbourne	Australia	Australia	131	Washington	United States	North America
60	Sydney	Australia	Australia	132	Buenos Aires	Argentina	South America
61	Vienna	Austria	Europe	133	La Paz	Bolivia	South America
62	Minsk	Belarus	Europe	134	Santa Cruz	Bolivia	South America
63	Brussels	Belgium	Europe	135	Belo Horizonte	Brazil	South America
64	Sofia	Bulgaria	Europe	136	Brasilia	Brazil	South America
65	Zagreb	Croatia	Europe	137	Fortaleza	Brazil	South America
66	Prague	Czechia	Europe	138	Rio de Janeiro	Brazil	South America
67	Paris	France	Europe	139	Sao Paulo	Brazil	South America
68	Berlin	Germany	Europe	140	Santiago	Chile	South America
69	Cologne	Germany	Europe	141	Bogota	Colombia	South America
70	Hamburg	Germany	Europe	142	Medellin	Colombia	South America
71	Munich	Germany	Europe	143	Quito	Ecuador	South America
72	Athens	Greece	Europe	144	Lima	Peru	South America

Supplementary Table 2. Pattern proportions of cities at small scale.

No.	City	Gridiron	Linear	Chaotic	Organic	Radial	Tributary	No.	City	Gridiron	Linear	Chaotic	Organic	Radial	Tributary
1	Algiers	10.1%	25.1%	28.5%	4.5%	5.0%	26.7%	73	Budapest	11.9%	22.6%	45.8%	0.2%	2.7%	16.8%
2	Luanda	19.2%	19.4%	50.9%	0.4%	0.9%	9.1%	74	Dublin	12.1%	15.2%	27.2%	4.7%	3.9%	36.8%
3	Kinshasa	16.4%	16.5%	55.8%	0.4%	0.9%	10.0%	75	Milan	2.8%	29.7%	45.8%	0.9%	2.5%	18.3%
4	Abidjan	9.0%	12.9%	70.0%	0.2%	0.8%	7.1%	76	Rome	7.3%	25.5%	36.8%	2.7%	5.9%	21.8%
5	Alexandria	5.3%	20.3%	61.3%	4.1%	3.3%	5.7%	77	Amsterdam	4.5%	24.6%	40.7%	1.2%	3.9%	25.2%
6	Cairo	21.1%	19.2%	33.1%	4.1%	7.5%	15.1%	78	The Hague	12.5%	29.8%	40.9%	0.7%	1.8%	14.3%
7	Addis Ababa	4.7%	20.0%	58.5%	2.5%	2.5%	11.9%	79	Oslo	14.1%	16.2%	32.3%	2.8%	6.0%	28.8%
8	Nairobi	5.1%	18.1%	70.6%	0.5%	0.9%	4.8%	80	Warsaw	7.7%	29.4%	38.3%	2.0%	4.3%	18.3%
9	Casablanca	11.5%	22.7%	34.0%	4.0%	4.7%	23.0%	81	Bucharest	6.0%	30.0%	41.1%	4.1%	4.0%	14.8%
10	Kano	4.8%	18.0%	70.6%	0.1%	0.3%	6.1%	82	Kazan	8.5%	29.8%	42.4%	1.0%	3.6%	14.7%
11	Johannesburg	5.0%	33.2%	40.4%	1.3%	2.5%	17.7%	83	Moscow	14.3%	24.4%	18.0%	5.6%	12.6%	25.1%
12	Khartoum	36.1%	13.0%	40.1%	0.1%	0.6%	10.1%	84	Nizhniy Novgorod	9.6%	18.3%	58.8%	0.7%	1.9%	10.8%
13	Omdurman	13.2%	9.2%	76.3%	0.0%	0.0%	1.3%	85	Perm	0.9%	23.7%	57.2%	3.6%	1.2%	13.4%
14	Dar es Salaam	3.1%	23.4%	67.5%	0.0%	0.5%	5.5%	86	Rostov	6.0%	23.9%	52.6%	1.7%	1.9%	13.9%
15	Dhaka	1.8%	16.8%	71.8%	1.0%	0.8%	7.9%	87	Saint Petersburg	17.2%	19.2%	18.1%	9.8%	5.6%	30.1%
16	Baoding	0.5%	40.5%	49.5%	0.0%	1.4%	8.2%	88	Samara	2.9%	21.3%	63.2%	2.1%	0.8%	9.7%
17	Beijing	2.7%	39.1%	13.8%	0.2%	4.1%	40.2%	89	Ufa	1.8%	14.1%	70.9%	1.7%	1.8%	9.5%
18	Changchun	0.2%	38.7%	50.6%	0.0%	0.7%	9.8%	90	Volgograd	2.1%	24.3%	65.0%	0.8%	1.6%	6.2%
19	Changsha	1.3%	40.8%	22.5%	1.9%	3.4%	30.0%	91	Voronezh	7.1%	25.9%	55.2%	0.1%	1.7%	10.0%
20	Chengdu	5.2%	35.9%	22.4%	2.2%	8.7%	25.6%	92	Belgrade	8.4%	13.7%	58.9%	2.5%	2.0%	14.5%
21	Chongqing	1.1%	43.0%	28.8%	2.9%	3.8%	20.4%	93	Barcelona	14.5%	19.8%	43.2%	2.8%	2.9%	16.9%
22	Dongguan	1.1%	42.9%	39.7%	0.9%	3.9%	11.6%	94	Madrid	11.0%	22.4%	32.4%	3.2%	9.2%	21.9%
23	Fuzhou	0.1%	35.9%	44.8%	1.2%	2.6%	15.3%	95	Sevilla	3.5%	26.4%	52.3%	2.4%	3.6%	11.8%
24	Ganzhou	0.6%	27.6%	55.0%	1.3%	1.0%	14.5%	96	Dnipro	1.8%	26.2%	59.4%	1.3%	2.5%	8.8%
25	Guangzhou	1.5%	40.4%	30.2%	2.0%	3.6%	22.3%	97	Kyiv	5.3%	28.3%	43.0%	1.3%	3.5%	18.6%
26	Hangzhou	0.8%	31.3%	21.7%	6.8%	4.5%	34.9%	98	Odesa	5.2%	30.1%	44.0%	1.3%	1.1%	18.3%
27	Hefei	1.3%	36.9%	22.1%	2.9%	5.5%	31.3%	99	Birmingham	8.5%	21.4%	24.8%	2.8%	6.0%	36.5%
28	Jinan	1.7%	28.2%	32.7%	3.5%	5.0%	28.9%	100	Birstall	3.1%	20.4%	64.4%	0.2%	0.8%	11.1%
29	Nanchang	0.2%	47.2%	28.5%	1.5%	3.0%	19.5%	101	Leeds	11.9%	26.4%	38.6%	0.6%	5.3%	17.2%
30	Nanjing	0.7%	41.1%	27.2%	4.5%	3.9%	22.6%	102	London	6.1%	10.3%	5.7%	14.2%	6.5%	57.3%
31	Nanyang	1.4%	37.8%	50.8%	0.4%	1.2%	8.3%	103	Manchester	5.7%	23.5%	27.3%	4.1%	5.5%	33.8%
32	Ningbo	0.8%	36.6%	23.5%	7.1%	3.5%	28.5%	104	Newcastle	7.2%	25.6%	39.2%	2.6%	3.3%	22.2%
33	Qingdao	1.9%	34.9%	27.1%	2.3%	3.5%	30.3%	105	Montreal	24.0%	16.8%	22.8%	5.2%	8.6%	22.5%
34	Shanghai	1.0%	33.4%	11.0%	3.9%	10.0%	40.7%	106	Toronto	4.7%	17.6%	20.9%	3.3%	3.6%	49.9%
35	Shenyang	1.6%	43.2%	32.8%	2.3%	1.3%	18.8%	107	Vancouver	42.5%	12.1%	27.2%	0.4%	2.0%	15.8%
36	Shenzhen	4.4%	27.1%	40.4%	4.1%	7.0%	17.1%	108	Santo Domingo	14.8%	23.1%	41.2%	3.1%	3.7%	14.1%
37	Shijiazhuang	0.2%	45.8%	33.1%	0.5%	1.1%	19.3%	109	Guatemala City	5.0%	21.2%	63.3%	2.2%	1.5%	6.8%
38	Tianjin	1.2%	46.5%	24.3%	2.5%	3.5%	22.0%	110	Guadalajara	22.6%	24.6%	36.7%	0.8%	4.8%	10.5%
39	Wuhan	0.7%	46.7%	20.3%	2.8%	4.0%	25.4%	111	Mexico City	33.6%	7.7%	16.5%	23.6%	14.0%	4.5%
40	Xi'an	8.8%	25.5%	29.3%	4.2%	8.4%	23.8%	112	Monterrey	33.0%	14.6%	33.6%	1.5%	5.1%	12.2%
41	Delhi	14.9%	27.3%	37.9%	2.3%	2.0%	15.5%	113	Tijuana	20.8%	17.6%	43.4%	1.1%	3.7%	13.5%
42	Kolkata	11.0%	22.2%	51.2%	2.6%	1.3%	11.8%	114	Atlanta	9.3%	24.2%	46.6%	1.2%	3.3%	15.4%
43	Jakarta	30.3%	18.0%	19.9%	2.2%	9.8%	19.8%	115	Boston	27.5%	14.5%	20.3%	5.6%	6.3%	25.8%
44	Tehran	30.1%	9.2%	10.5%	21.3%	11.0%	17.9%	116	Chicago	61.3%	9.3%	7.7%	2.0%	5.1%	14.6%
45	Nagoya	19.0%	15.8%	15.7%	2.9%	5.8%	40.9%	117	Dallas	29.9%	24.2%	19.3%	2.4%	7.2%	17.0%
46	Osaka	33.8%	11.3%	18.2%	2.1%	7.8%	26.9%	118	Denver	36.0%	18.5%	29.2%	0.6%	3.0%	12.6%
47	Tokyo	39.2%	7.3%	4.4%	6.2%	6.2%	36.7%	119	Detroit	41.3%	11.8%	14.9%	2.6%	10.8%	18.6%
48	Seoul	9.4%	17.7%	21.6%	19.6%	7.6%	24.1%	120	Houston	23.1%	20.9%	13.7%	3.9%	14.4%	25.0%
49	Kuala Lumpur	19.4%	17.8%	40.9%	1.7%	4.0%	16.2%	121	Los Angeles	37.0%	8.5%	24.5%	9.6%	6.2%	14.3%
50	Karachi	26.6%	19.7%	32.2%	5.6%	4.5%	11.4%	122	Miami	31.4%	20.8%	16.7%	0.9%	4.2%	25.9%
51	Lahore	20.0%	18.3%	39.9%	2.9%	5.7%	13.1%	123	Minneapolis	54.0%	12.3%	18.6%	0.9%	4.0%	10.3%
52	Manila	20.7%	19.6%	16.8%	7.3%	7.5%	28.1%	124	New York	17.5%	12.6%	15.3%	8.3%	12.1%	34.1%
53	Singapore	3.6%	33.9%	26.5%	5.8%	7.3%	22.9%	125	Philadelphia	25.0%	19.1%	18.1%	3.8%	7.7%	26.3%
54	Bangkok	16.4%	29.1%	32.0%	1.2%	6.9%	14.4%	126	Phoenix	34.9%	16.1%	22.0%	0.8%	4.1%	22.2%
55	Istanbul	31.4%	13.1%	9.1%	13.2%	12.6%	20.5%	127	San Diego	16.4%	21.5%	45.1%	2.0%	4.5%	10.5%
56	Hanoi	8.6%	30.8%	44.3%	1.3%	5.6%	9.4%	128	San Francisco	25.0%	20.4%	30.0%	3.0%	7.3%	14.3%
57	Ho Chi Minh City	17.8%	17.4%	49.0%	2.0%	4.4%	9.4%	129	Seattle	50.5%	12.7%	16.8%	1.1%	3.5%	15.4%
58	Brisbane	3.8%	29.4%	35.6%	2.2%	3.0%	26.1%	130	Tampa	17.1%	27.2%	42.8%	0.5%	1.6%	10.8%
59	Melbourne	18.9%	19.6%	13.9%	2.1%	7.6%	37.9%	131	Washington	22.6%	25.6%	20.5%	2.0%	5.9%	23.4%
60	Sydney	6.0%	22.4%	31.4%	4.2%	4.4%	31.8%	132	Buenos Aires	9.3%	16.4%	14.0%	10.0%	10.2%	40.2%
61	Vienna	5.8%	27.7%	34.0%	3.0%	6.4%	23.0%	133	La Paz	18.5%	14.6%	55.2%	2.4%	3.0%	6.3%
62	Minsk	4.7%	30.7%	26.2%	3.2%	4.1%	31.1%	134	Santa Cruz	11.4%	14.0%	62.7%	1.2%	4.1%	6.6%
63	Brussels	6.3%	23.6%	38.7%	2.1%	5.7%	23.6%	135	Belo Horizonte	20.2%	14.7%	49.2%	1.4%	6.2%	8.4%
64	Sofia	6.1%	23.1%	56.4%	1.3%	3.3%	9.8%	136	Brasilia	5.2%	25.7%	54.4%	3.3%	6.5%	4.9%
65	Zagreb	12.4%	15.1%	58.6%	0.8%	0.4%	12.7%	137	Fortaleza	17.3%	30.7%	28.9%	3.5%	4.8%	14.8%
66	Prague	6.7%	23.4%	41.6%	1.8%	3.6%	22.9%	138	Rio de Janeiro	9.5%	18.9%	47.0%	2.7%	8.0%	13.8%
67	Paris	6.8%	10.7%	5.8%	15.3%	13.2%	48.3%	139	Sao Paulo	32.7%	12.1%	8.0%	7.0%	16.0%	24.3%
68	Berlin	6.1%	24.8%	17.3%	4.1%	5.6%	42.0%	140	Santiago	21.5%	10.2%	15.9%	10.5%	15.6%	26.2%
69	Cologne	4.4%	28.1%	34.8%	2.4%	4.4%	25.8%	141	Bogota	16.1%	12.4%	52.1%	3.8%	9.9%	5.7%
70	Hamburg	3.7%	22.3%	36.0%	2.8%	5.2%	30.0%	142	Medellin	8.6%	12.5%	70.5%	1.4%	1.7%	5.3%
71	Munich	4.6%	26.8%	36.2%	2.0%	2.7%	27.8%	143	Quito	5.3%	16.3%	66.7%	1.6%	2.2%	7.8%
72	Athens	39.1%	12.7%	30.4%	2.0%	6.2%	9.7%	144	Lima	16.6%	11.2%	32.1%	11.6%	12.7%	15.9%

Supplementary Table 3. Pattern proportions of cities at mid scale.

No.	City	Gridiron	Linear	Chaotic	Organic	Radial	Tributary	No.	City	Gridiron	Linear	Chaotic	Organic	Radial	Tributary
1	Algiers	2.8%	14.4%	11.6%	19.4%	14.7%	37.0%	73	Budapest	21.5%	12.1%	22.9%	7.0%	8.4%	28.1%
2	Luanda	37.0%	14.2%	18.2%	3.8%	4.2%	22.6%	74	Dublin	18.1%	7.9%	12.9%	12.6%	14.9%	33.7%
3	Kinshasa	18.2%	12.9%	39.9%	4.2%	3.1%	21.7%	75	Milan	5.4%	16.5%	23.9%	6.1%	7.8%	40.4%
4	Abidjan	15.4%	12.5%	53.6%	2.0%	2.4%	14.0%	76	Rome	5.9%	16.2%	16.4%	11.5%	14.7%	35.3%
5	Alexandria	0.8%	16.9%	52.5%	14.2%	3.9%	11.7%	77	Amsterdam	2.9%	14.2%	27.4%	14.6%	9.3%	31.6%
6	Cairo	11.8%	9.8%	19.9%	26.0%	12.9%	19.5%	78	The Hague	13.5%	18.2%	19.6%	5.5%	10.1%	33.1%
7	Addis Ababa	2.0%	13.0%	46.2%	11.9%	4.6%	22.3%	79	Oslo	10.3%	4.7%	22.0%	13.3%	17.7%	32.0%
8	Nairobi	8.1%	20.2%	51.5%	2.2%	2.0%	15.9%	80	Warsaw	3.3%	11.1%	18.9%	18.0%	11.1%	37.6%
9	Casablanca	4.3%	12.5%	18.9%	27.4%	9.1%	27.7%	81	Bucharest	3.0%	25.8%	20.0%	17.5%	6.0%	27.7%
10	Kano	5.9%	19.8%	51.4%	1.7%	2.1%	19.1%	82	Kazan	7.6%	18.5%	22.1%	12.1%	7.1%	32.6%
11	Johannesburg	8.4%	16.8%	14.3%	5.9%	10.0%	44.6%	83	Moscow	7.1%	1.7%	6.9%	31.4%	22.6%	30.2%
12	Khartoum	41.2%	7.0%	29.2%	1.7%	3.0%	17.9%	84	Nizhniy Novgorod	11.0%	14.3%	39.8%	2.5%	6.5%	26.0%
13	Omdurman	16.8%	14.4%	63.2%	0.0%	0.3%	5.2%	85	Perm	0.5%	20.7%	40.9%	10.1%	4.8%	23.0%
14	Dar es Salaam	10.5%	18.6%	43.9%	0.9%	2.4%	23.7%	86	Rostov	8.5%	22.0%	34.2%	8.9%	6.4%	20.1%
15	Dhaka	2.0%	17.0%	58.6%	6.6%	2.0%	14.0%	87	Saint Petersburg	4.4%	1.9%	7.5%	46.7%	11.4%	28.1%
16	Baoding	0.3%	35.6%	25.2%	1.7%	1.2%	36.0%	88	Samara	6.5%	16.7%	51.4%	5.2%	3.9%	16.2%
17	Beijing	6.0%	6.2%	2.2%	29.5%	7.1%	49.0%	89	Ufa	3.1%	18.1%	58.2%	5.7%	3.8%	11.0%
18	Changchun	0.9%	22.2%	29.2%	3.7%	5.0%	39.0%	90	Volgograd	2.1%	18.8%	51.1%	3.8%	2.7%	21.5%
19	Changsha	2.6%	11.1%	7.1%	30.3%	4.4%	44.6%	91	Voronezh	5.0%	20.0%	35.8%	3.8%	6.4%	29.0%
20	Chengdu	4.9%	10.2%	7.0%	26.5%	10.8%	40.5%	92	Belgrade	8.3%	10.6%	48.4%	11.4%	4.8%	16.6%
21	Chongqing	0.8%	16.6%	9.1%	24.2%	7.2%	42.1%	93	Barcelona	12.9%	14.9%	26.7%	10.3%	12.1%	23.0%
22	Dongguan	0.3%	16.6%	19.0%	14.9%	6.0%	43.3%	94	Madrid	8.6%	10.8%	20.2%	17.6%	17.3%	25.5%
23	Fuzhou	0.0%	19.8%	28.3%	18.3%	4.3%	29.3%	95	Sevilla	0.7%	25.8%	36.8%	10.6%	5.6%	20.5%
24	Ganzhou	0.7%	14.1%	42.8%	12.3%	2.4%	27.8%	96	Dnipro	5.3%	19.9%	37.9%	4.4%	3.4%	29.0%
25	Guangzhou	2.3%	12.4%	12.3%	21.5%	4.9%	46.5%	97	Kyiv	5.2%	10.8%	21.7%	7.1%	12.5%	42.7%
26	Hangzhou	1.5%	13.6%	8.6%	50.2%	3.7%	22.4%	98	Odesa	8.5%	29.0%	21.1%	8.2%	5.4%	27.8%
27	Hefei	2.3%	8.4%	8.4%	36.7%	4.2%	39.8%	99	Birmingham	15.0%	2.0%	3.5%	16.2%	21.2%	42.0%
28	Jinan	3.0%	16.0%	18.3%	28.5%	7.6%	26.8%	100	Birstall	3.3%	12.4%	52.4%	2.2%	4.2%	25.4%
29	Nanchang	0.0%	19.3%	5.4%	19.4%	6.0%	49.8%	101	Leeds	8.1%	15.3%	17.8%	5.8%	13.2%	39.8%
30	Nanjing	0.8%	11.6%	12.9%	27.8%	6.1%	40.7%	102	London	0.9%	0.4%	0.4%	58.5%	20.1%	19.7%
31	Nanyang	1.2%	37.9%	30.0%	8.7%	1.9%	20.3%	103	Manchester	6.7%	5.6%	9.2%	21.7%	16.7%	40.2%
32	Ningbo	0.4%	13.4%	7.6%	37.2%	3.8%	37.5%	104	Newcastle	3.0%	13.5%	23.7%	13.2%	9.0%	37.6%
33	Qingdao	2.1%	13.3%	9.8%	30.3%	5.6%	38.8%	105	Montreal	20.3%	3.4%	9.0%	24.6%	19.5%	23.1%
34	Shanghai	1.1%	3.2%	0.5%	46.3%	10.8%	38.1%	106	Toronto	2.9%	1.6%	1.8%	11.5%	14.2%	67.9%
35	Shenyang	1.6%	19.5%	12.7%	17.3%	3.4%	45.5%	107	Vancouver	51.1%	8.7%	15.8%	6.4%	3.9%	14.0%
36	Shenzhen	2.4%	17.2%	25.8%	22.8%	9.8%	22.0%	108	Santo Domingo	12.8%	18.1%	26.4%	11.0%	6.7%	25.1%
37	Shijiazhuang	1.2%	20.9%	11.5%	10.9%	5.1%	50.5%	109	Guatemala City	2.0%	18.3%	50.1%	6.1%	4.1%	19.4%
38	Tianjin	1.7%	13.4%	6.7%	27.4%	5.0%	45.7%	110	Guadalajara	23.3%	11.8%	21.5%	7.3%	10.6%	25.6%
39	Wuhan	0.4%	11.1%	4.6%	33.8%	6.2%	44.0%	111	Mexico City	8.0%	1.8%	7.6%	71.3%	6.3%	5.1%
40	Xi'an	11.1%	7.9%	14.3%	31.3%	10.5%	24.9%	112	Monterrey	24.3%	3.9%	26.2%	8.9%	13.8%	22.9%
41	Delhi	14.0%	12.1%	16.9%	11.2%	10.0%	35.8%	113	Tijuana	21.2%	8.9%	29.9%	8.0%	7.3%	24.7%
42	Kolkata	8.2%	17.5%	35.0%	11.7%	4.7%	22.9%	114	Atlanta	15.1%	16.6%	21.8%	2.9%	9.6%	34.1%
43	Jakarta	30.3%	3.3%	5.3%	12.1%	18.1%	31.0%	115	Boston	21.5%	5.3%	8.5%	20.0%	18.0%	26.7%
44	Tehran	12.8%	2.4%	5.7%	59.8%	12.6%	6.6%	116	Chicago	72.6%	1.4%	2.2%	6.1%	6.5%	11.2%
45	Nagoya	22.5%	2.8%	3.6%	23.0%	13.4%	34.6%	117	Dallas	24.7%	7.8%	6.2%	13.9%	14.7%	32.8%
46	Osaka	31.8%	4.2%	8.4%	19.4%	13.2%	23.1%	118	Denver	46.4%	6.9%	14.1%	3.9%	6.3%	22.5%
47	Tokyo	26.3%	0.6%	0.6%	37.9%	20.5%	14.0%	119	Detroit	45.3%	1.9%	4.0%	11.7%	16.4%	20.6%
48	Seoul	3.8%	5.9%	11.1%	47.2%	12.9%	19.1%	120	Houston	21.5%	3.0%	0.8%	21.3%	28.2%	25.2%
49	Kuala Lumpur	15.7%	6.6%	28.0%	10.3%	10.8%	28.6%	121	Los Angeles	37.6%	4.1%	12.9%	24.6%	11.5%	9.4%
50	Karachi	11.4%	13.1%	20.5%	25.8%	9.7%	19.7%	122	Miami	52.9%	10.6%	5.9%	7.0%	9.2%	14.4%
51	Lahore	18.2%	8.1%	24.0%	12.2%	12.0%	25.5%	123	Minneapolis	66.1%	3.5%	5.0%	3.7%	6.7%	15.0%
52	Manila	12.6%	5.7%	6.3%	35.0%	12.6%	27.8%	124	New York	16.9%	3.1%	10.1%	27.8%	25.6%	16.4%
53	Singapore	0.4%	13.4%	15.7%	33.8%	11.8%	25.0%	125	Philadelphia	18.1%	7.8%	4.3%	17.1%	22.8%	30.0%
54	Bangkok	14.3%	10.4%	11.6%	6.8%	13.0%	43.9%	126	Phoenix	61.2%	6.0%	7.0%	1.6%	5.4%	18.8%
55	Istanbul	9.0%	4.5%	2.1%	45.0%	22.4%	17.0%	127	San Diego	14.5%	14.2%	27.5%	4.3%	12.1%	27.4%
56	Hanoi	5.3%	22.3%	22.9%	7.6%	9.4%	32.4%	128	San Francisco	24.0%	11.1%	17.2%	12.2%	15.2%	20.3%
57	Ho Chi Minh City	20.7%	10.8%	31.8%	6.9%	9.6%	20.2%	129	Seattle	64.2%	3.6%	8.4%	3.0%	5.4%	15.4%
58	Brisbane	6.1%	15.9%	14.7%	9.5%	10.0%	43.8%	130	Tampa	33.7%	15.6%	16.5%	1.1%	4.0%	29.0%
59	Melbourne	21.7%	4.1%	2.0%	21.3%	17.0%	34.0%	131	Washington	17.9%	4.9%	4.8%	14.8%	20.9%	36.7%
60	Sydney	4.7%	9.2%	16.8%	21.7%	12.1%	35.4%	132	Buenos Aires	11.0%	3.8%	7.3%	40.1%	20.1%	17.7%
61	Vienna	5.1%	13.5%	16.2%	15.0%	17.4%	32.8%	133	La Paz	12.5%	13.6%	46.2%	7.7%	7.1%	12.9%
62	Minsk	2.1%	9.3%	9.3%	31.0%	7.2%	41.2%	134	Santa Cruz	17.9%	10.1%	48.4%	7.4%	5.9%	10.2%
63	Brussels	4.0%	12.4%	20.2%	10.9%	15.3%	37.2%	135	Belo Horizonte	22.4%	10.1%	35.6%	4.8%	13.0%	14.2%
64	Sofia	5.0%	14.6%	42.4%	5.8%	6.7%	25.5%	136	Brasilia	2.4%	20.7%	41.2%	8.0%	11.7%	16.1%
65	Zagreb	15.6%	14.3%	42.4%	2.0%	3.0%	22.8%	137	Fortaleza	12.4%	14.7%	10.1%	14.7%	13.7%	34.5%
66	Prague	2.5%	11.0%	21.7%	13.0%	12.8%	39.0%	138	Rio de Janeiro	3.6%	13.9%	35.9%	11.0%	16.4%	19.3%
67	Paris	1.6%	0.6%	1.2%	48.4%	29.8%	18.3%	139	Sao Paulo	19.1%	0.9%	3.9%	30.6%	26.0%	19.6%
68	Berlin	4.4%	3.3%	3.5%	30.1%	17.9%	40.7%	140	Santiago	13.5%	3.4%	10.6%	39.8%	20.1%	12.7%
69	Cologne	4.4%	12.3%	15.0%	12.3%	9.3%	46.6%	141	Bogota	5.8%	8.0%	46.5%	21.7%	8.9%	9.1%
70	Hamburg	4.2%	11.6%	16.2%	19.2%	12.3%	36.6%	142	Medellin	6.6%	16.0%	61.0%	6.0%	4.5%	6.0%
71	Munich	2.6%	13.9%	16.5%	19.4%	11.9%	35.7%	143	Quito	6.6%	10.0%	56.6%	6.4%	6.0%	14.4%
72	Athens	26.4%	7.4%	23.4%	14.1%	14.3%	14.3%	144	Lima	6.0%	4.2%	24.2%	43.8%	11.0%	10.7%

Supplementary Table 4. Pattern proportions of cities at large scale.

No.	City	Gridiron	Linear	Chaotic	Organic	Radial	Tributary	No.	City	Gridiron	Linear	Chaotic	Organic	Radial	Tributary
1	Algiers	5.0%	6.3%	5.0%	28.8%	10.0%	45.0%	73	Budapest	31.3%	3.1%	18.8%	8.6%	12.5%	25.8%
2	Luanda	43.0%	10.3%	13.1%	7.5%	4.7%	21.5%	74	Dublin	47.5%	3.0%	11.9%	9.9%	9.9%	17.8%
3	Kinshasa	24.4%	10.4%	31.9%	3.7%	3.7%	25.9%	75	Milan	12.6%	8.1%	11.9%	8.1%	12.6%	46.7%
4	Abidjan	23.2%	11.0%	43.3%	3.0%	3.0%	16.5%	76	Rome	8.6%	7.2%	7.2%	20.1%	12.9%	43.9%
5	Alexandria	1.1%	17.0%	45.7%	16.0%	3.2%	17.0%	77	Amsterdam	15.0%	4.4%	23.9%	21.2%	9.7%	25.7%
6	Cairo	14.9%	4.8%	14.3%	33.3%	8.9%	23.8%	78	The Hague	18.4%	11.5%	14.9%	6.9%	10.3%	37.9%
7	Addis Ababa	5.5%	12.6%	41.2%	14.3%	3.8%	22.5%	79	Oslo	26.7%	4.0%	17.3%	16.0%	18.7%	17.3%
8	Nairobi	15.7%	13.6%	39.3%	1.6%	1.6%	28.3%	80	Warsaw	11.3%	7.0%	11.3%	27.0%	15.7%	27.8%
9	Casablanca	7.3%	4.9%	14.6%	30.5%	18.3%	24.4%	81	Bucharest	6.8%	18.0%	12.8%	22.6%	6.0%	33.8%
10	Kano	10.2%	17.7%	45.7%	3.2%	1.1%	22.0%	82	Kazan	20.0%	10.6%	14.1%	11.8%	11.8%	31.8%
11	Johannesburg	12.9%	4.7%	7.1%	5.9%	11.8%	57.6%	83	Moscow	15.2%	0.0%	1.9%	41.0%	17.1%	17.1%
12	Khartoum	50.6%	7.8%	23.4%	3.9%	1.3%	13.0%	84	Nizhniy Novgorod	20.0%	6.0%	39.0%	1.0%	11.0%	23.0%
13	Omdurman	17.7%	20.3%	60.8%	0.0%	0.0%	1.3%	85	Perm	2.0%	11.1%	36.4%	11.1%	8.1%	31.3%
14	Dar es Salaam	32.5%	8.8%	24.6%	0.9%	5.3%	28.1%	86	Rostov	12.2%	13.0%	27.5%	9.9%	4.6%	32.8%
15	Dhaka	4.8%	7.1%	60.1%	8.3%	1.8%	17.9%	87	Saint Petersburg	14.4%	1.1%	3.3%	46.7%	15.6%	18.9%
16	Baoding	0.7%	21.9%	19.9%	6.2%	4.1%	47.3%	88	Samara	11.1%	11.1%	49.5%	11.1%	0.0%	17.2%
17	Beijing	13.1%	2.1%	0.7%	55.2%	6.9%	22.1%	89	Ufa	11.1%	18.5%	53.7%	6.5%	3.7%	6.5%
18	Changchun	1.5%	16.9%	25.0%	10.3%	4.4%	41.9%	90	Volgograd	4.1%	18.2%	43.8%	3.3%	4.1%	26.4%
19	Changsha	7.2%	3.0%	5.4%	46.4%	4.8%	33.1%	91	Voronezh	8.5%	10.4%	33.0%	0.9%	10.4%	36.8%
20	Chengdu	2.4%	3.7%	2.4%	52.4%	7.3%	31.7%	92	Belgrade	20.8%	7.7%	43.1%	10.0%	5.4%	13.1%
21	Chongqing	0.6%	10.4%	6.1%	44.5%	4.9%	33.5%	93	Barcelona	14.9%	10.3%	24.1%	9.2%	14.9%	26.4%
22	Dongguan	0.6%	12.6%	13.1%	29.7%	8.0%	36.0%	94	Madrid	11.1%	4.9%	15.3%	22.9%	16.0%	29.9%
23	Fuzhou	0.0%	13.0%	25.4%	31.4%	3.0%	27.2%	95	Sevilla	1.4%	15.0%	34.0%	14.3%	5.4%	29.9%
24	Ganzhou	0.6%	4.7%	42.0%	21.3%	3.6%	27.8%	96	Dnipro	11.0%	15.3%	28.0%	7.6%	6.8%	31.4%
25	Guangzhou	3.5%	4.6%	5.2%	34.1%	6.4%	46.2%	97	Kyiv	14.2%	7.5%	13.3%	5.8%	21.7%	37.5%
26	Hangzhou	3.2%	6.5%	6.5%	55.2%	7.1%	21.4%	98	Odesa	15.7%	16.9%	12.0%	4.8%	9.6%	41.0%
27	Hefei	5.0%	3.1%	6.3%	56.9%	2.5%	26.3%	99	Birmingham	25.7%	0.9%	0.0%	25.7%	24.8%	23.0%
28	Jinan	5.3%	9.2%	15.8%	39.5%	8.6%	21.7%	100	Birstall	8.0%	10.6%	45.1%	2.7%	8.8%	24.8%
29	Nanchang	0.6%	6.6%	1.8%	38.0%	4.8%	48.2%	101	Leeds	10.2%	7.4%	13.9%	13.0%	12.0%	43.5%
30	Nanjing	0.7%	6.0%	9.3%	48.3%	8.6%	27.2%	102	London	6.8%	0.0%	0.0%	71.8%	16.2%	5.1%
31	Nanyang	0.6%	21.7%	31.1%	12.4%	0.0%	34.2%	103	Manchester	12.5%	1.8%	5.4%	24.1%	16.1%	40.2%
32	Ningbo	1.2%	7.1%	2.9%	52.4%	5.9%	30.6%	104	Newcastle	7.4%	5.6%	17.6%	19.4%	9.3%	40.7%
33	Qingdao	5.3%	10.6%	4.3%	44.7%	9.6%	25.5%	105	Montreal	30.8%	1.7%	6.0%	30.8%	17.1%	13.7%
34	Shanghai	0.6%	0.0%	0.0%	73.5%	6.2%	19.8%	106	Toronto	29.2%	0.0%	0.7%	12.4%	10.2%	47.4%
35	Shenyang	0.7%	13.6%	5.0%	30.7%	5.7%	44.3%	107	Vancouver	58.7%	4.6%	10.1%	8.3%	3.7%	14.7%
36	Shenzhen	1.3%	14.6%	19.0%	31.6%	14.6%	19.0%	108	Santo Domingo	18.6%	14.2%	20.4%	13.3%	7.1%	26.5%
37	Shijiazhuang	0.7%	9.9%	6.6%	23.0%	7.2%	52.6%	109	Guatemala City	4.9%	10.8%	40.5%	8.1%	5.4%	30.3%
38	Tianjin	0.7%	7.6%	1.4%	42.8%	9.7%	37.9%	110	Guadalajara	23.7%	5.6%	18.6%	13.0%	11.3%	27.7%
39	Wuhan	0.7%	2.8%	4.2%	56.3%	9.2%	26.8%	111	Mexico City	9.3%	0.0%	6.0%	73.6%	7.1%	3.8%
40	Xi'an	27.7%	4.4%	8.8%	36.5%	5.7%	17.0%	112	Monterrey	25.8%	1.3%	25.2%	16.1%	16.8%	14.8%
41	Delhi	16.7%	6.6%	13.7%	17.9%	10.7%	35.1%	113	Tijuana	33.6%	4.2%	23.1%	9.1%	7.7%	22.4%
42	Kolkata	13.3%	11.0%	31.2%	12.1%	4.0%	28.3%	114	Atlanta	38.9%	3.2%	11.5%	0.6%	7.0%	38.9%
43	Jakarta	39.4%	1.7%	2.2%	14.4%	15.0%	27.2%	115	Boston	31.5%	0.8%	7.3%	19.4%	17.7%	23.4%
44	Tehran	23.9%	0.6%	3.2%	59.4%	7.1%	5.8%	116	Chicago	91.1%	0.0%	0.0%	2.4%	4.1%	2.4%
45	Nagoya	37.3%	2.0%	2.0%	26.8%	13.7%	18.3%	117	Dallas	36.7%	1.9%	2.5%	20.9%	11.4%	26.6%
46	Osaka	45.2%	1.9%	5.2%	24.5%	13.5%	9.7%	118	Denver	56.3%	2.1%	14.6%	4.9%	2.8%	19.4%
47	Tokyo	35.9%	0.0%	0.0%	44.9%	16.0%	3.2%	119	Detroit	67.1%	0.0%	0.7%	13.3%	7.7%	11.2%
48	Seoul	13.1%	2.0%	9.2%	56.2%	5.9%	13.7%	120	Houston	39.0%	0.0%	0.0%	28.0%	18.3%	14.6%
49	Kuala Lumpur	26.3%	2.1%	22.6%	15.3%	8.9%	24.7%	121	Los Angeles	41.6%	2.2%	19.0%	19.0%	10.2%	8.0%
50	Karachi	13.5%	9.0%	15.0%	32.3%	9.0%	21.1%	122	Miami	68.5%	5.4%	2.7%	5.4%	7.2%	10.8%
51	Lahore	25.0%	5.1%	23.7%	18.6%	9.6%	17.9%	123	Minneapolis	77.8%	0.7%	2.2%	3.7%	7.4%	8.1%
52	Manila	30.2%	0.9%	3.4%	34.5%	14.7%	16.4%	124	New York	35.8%	2.2%	8.0%	29.9%	17.5%	6.6%
53	Singapore	0.7%	6.7%	8.2%	50.0%	8.2%	26.1%	125	Philadelphia	35.2%	4.1%	1.4%	17.2%	19.3%	22.8%
54	Bangkok	20.3%	5.3%	1.1%	14.4%	16.6%	42.2%	126	Phoenix	80.4%	2.5%	5.7%	0.6%	1.3%	9.5%
55	Istanbul	12.3%	0.9%	0.9%	52.8%	21.7%	11.3%	127	San Diego	24.1%	5.7%	20.3%	4.4%	10.1%	35.4%
56	Hanoi	6.7%	13.5%	13.5%	11.2%	10.1%	44.9%	128	San Francisco	35.1%	8.1%	13.5%	13.5%	9.5%	20.3%
57	Ho Chi Minh City	25.5%	7.4%	22.3%	9.6%	10.6%	24.5%	129	Seattle	85.5%	1.2%	4.8%	0.0%	2.4%	6.0%
58	Brisbane	14.3%	7.1%	7.7%	12.5%	13.1%	45.2%	130	Tampa	49.7%	5.2%	9.7%	0.6%	1.9%	32.9%
59	Melbourne	37.5%	0.8%	1.6%	29.7%	10.9%	19.5%	131	Washington	31.3%	0.7%	2.7%	16.3%	23.8%	25.2%
60	Sydney	14.1%	4.7%	13.3%	24.2%	14.8%	28.9%	132	Buenos Aires	20.9%	2.3%	3.5%	48.8%	15.1%	9.3%
61	Vienna	9.4%	6.3%	11.7%	22.7%	18.0%	32.0%	133	La Paz	9.9%	7.6%	48.8%	11.0%	6.4%	16.3%
62	Minsk	11.1%	3.7%	6.5%	31.5%	13.0%	34.3%	134	Santa Cruz	20.9%	9.9%	44.5%	10.4%	4.9%	9.3%
63	Brussels	10.1%	5.9%	14.3%	21.8%	14.3%	33.6%	135	Belo Horizonte	24.7%	11.2%	29.8%	8.4%	11.8%	14.0%
64	Sofia	5.0%	12.2%	38.8%	9.4%	7.2%	27.3%	136	Brasilia	2.9%	12.0%	35.4%	11.4%	9.7%	28.6%
65	Zagreb	28.9%	8.1%	37.0%	1.5%	0.7%	23.7%	137	Fortaleza	12.2%	7.1%	6.1%	20.4%	9.2%	44.9%
66	Prague	6.6%	6.6%	18.2%	12.4%	19.0%	37.2%	138	Rio de Janeiro	6.3%	8.9%	25.9%	21.4%	13.4%	24.1%
67	Paris	10.5%	0.0%	0.8%	54.8%	26.6%	7.3%	139	Sao Paulo	24.6%	0.0%	2.3%	40.6%	21.1%	11.4%
68	Berlin	18.6%	0.9%	0.9%	39.8%	15.9%	23.9%	140	Santiago	25.3%	0.0%	9.1%	44.2%	11.7%	9.7%
69	Cologne	13.6%	3.4%	9.3%	18.6%	11.0%	44.1%	141	Bogota	7.0%	5.4%	47.8%	27.4%	5.4%	7.0%
70	Hamburg	13.0%	1.9%	13.9%	21.3%	14.8%	35.2%	142	Medellin	8.9%	11.6%	61.1%	3.2%	6.8%	8.4%
71	Munich	9.5%	7.1%	13.5%	27.0%	6.3%	36.5%	143	Quito	8.1%	8.1%	51.9%	8.1%	5.4%	18.4%
72	Athens	31.9%	9.4%	21.0%	18.8%	9.4%	9.4%	144	Lima	11.7%	3.9%	17.5%	48.1%	9.1%	9.7%

Supplementary Table 5. Aggregated cross-scale mapping relations (counts and percentages).

Large	Mid	Count of Mapping Relations	Percentage	Mid	Small	Count of Mapping Relations	Percentage
Gridiron	Gridiron	30016	50.3%	Gridiron	Gridiron	20786	53.8%
	Linear	1184	2.0%		Linear	2053	5.3%
	Chaotic	4704	7.9%		Chaotic	8215	21.2%
	Organic	6148	10.3%		Organic	673	1.7%
	Radial	4712	7.9%		Radial	830	2.1%
	Tributary	12920	21.6%		Tributary	6111	15.8%
Linear	Gridiron	300	1.4%	Linear	Gridiron	406	1.1%
	Linear	12068	56.5%		Linear	19166	51.5%
	Chaotic	7044	33.0%		Chaotic	16649	44.7%
	Organic	36	0.2%		Organic	21	0.1%
	Radial	220	1.0%		Radial	328	0.9%
	Tributary	1696	7.9%		Tributary	650	1.7%
Chaotic	Gridiron	916	1.7%	Chaotic	Gridiron	853	1.2%
	Linear	4288	8.0%		Linear	1282	1.9%
	Chaotic	47124	87.8%		Chaotic	65949	96.4%
	Organic	56	0.1%		Organic	27	0.0%
	Radial	152	0.3%		Radial	32	0.0%
	Tributary	1148	2.1%		Tributary	261	0.4%
Organic	Gridiron	2432	3.4%	Organic	Gridiron	8061	14.9%
	Linear	776	1.1%		Linear	8289	15.4%
	Chaotic	308	0.4%		Chaotic	994	1.8%
	Organic	39956	55.9%		Organic	7342	13.6%
	Radial	10596	14.8%		Radial	5884	10.9%
	Tributary	17400	24.3%		Tributary	23430	43.4%
Radial	Gridiron	1460	4.9%	Radial	Gridiron	4822	15.4%
	Linear	1500	5.0%		Linear	6248	20.0%
	Chaotic	540	1.8%		Chaotic	1476	4.7%
	Organic	6304	21.1%		Organic	2181	7.0%
	Radial	11000	36.9%		Radial	7058	22.6%
	Tributary	9036	30.3%		Tributary	9435	30.2%
Tributary	Gridiron	3544	4.4%	Tributary	Gridiron	6323	7.3%
	Linear	17404	21.8%		Linear	36699	42.5%
	Chaotic	8684	10.9%		Chaotic	22411	25.9%
	Organic	1500	1.9%		Organic	182	0.2%
	Radial	4540	5.7%		Radial	1376	1.6%
	Tributary	44248	55.4%		Tributary	19457	22.5%

Supplementary Table 6. Pattern indicators (PDP, PDI, NSI) of cities of interest.

No.	City	Small PDP	Mid PDP	Large PDP	Small PDI	Mid PDI	Large PDI	Mid GNSI
1	Algiers	0.29	0.37	0.45	1.58	1.60	1.42	0.41
2	Luanda	0.51	0.37	0.43	1.26	1.55	1.53	0.54
3	Kinshasa	0.56	0.40	0.32	1.21	1.51	1.54	0.63
4	Abidjan	0.70	0.54	0.43	0.97	1.33	1.45	0.62
5	Alexandria	0.61	0.53	0.46	1.19	1.33	1.41	0.67
6	Cairo	0.33	0.26	0.33	1.62	1.73	1.63	0.45
7	Addis Ababa	0.58	0.46	0.41	1.22	1.43	1.53	0.64
8	Nairobi	0.71	0.52	0.39	0.92	1.32	1.42	0.56
9	Casablanca	0.34	0.28	0.30	1.56	1.64	1.39	0.52
10	Kano	0.71	0.51	0.46	0.89	1.29	1.33	0.61
11	Johannesburg	0.40	0.45	0.58	1.33	1.54	1.33	0.44
12	Khartoum	0.40	0.41	0.51	1.27	1.39	0.99	0.58
13	Omdurman	0.76	0.63	0.61	0.75	1.04	1.48	0.68
14	Dar es Salaam	0.67	0.44	0.32	0.90	1.38	1.23	0.52
15	Dhaka	0.72	0.59	0.60	0.89	1.22	1.35	0.68
16	Baoding	0.49	0.36	0.47	1.00	1.22	1.23	0.57
17	Beijing	0.40	0.49	0.42	1.25	1.32	1.45	0.55
18	Changchun	0.51	0.39	0.46	0.99	1.37	1.32	0.61
19	Changsha	0.41	0.45	0.52	1.31	1.38	1.20	0.54
20	Chengdu	0.36	0.41	0.45	1.50	1.53	1.31	0.48
21	Chongqing	0.43	0.42	0.36	1.32	1.45	1.49	0.52
22	Dongguan	0.43	0.43	0.31	1.20	1.44	1.44	0.52
23	Fuzhou	0.45	0.29	0.46	1.17	1.48	1.34	0.55
24	Ganzhou	0.55	0.43	0.46	1.10	1.38	1.31	0.63
25	Guangzhou	0.40	0.47	0.55	1.32	1.44	1.20	0.54
26	Hangzhou	0.35	0.50	0.57	1.42	1.35	1.37	0.60
27	Hefei	0.37	0.40	0.39	1.38	1.37	1.57	0.58
28	Jinan	0.33	0.50	0.48	1.42	1.61	1.15	0.51
29	Nanchang	0.47	0.41	0.34	1.21	1.31	1.34	0.54
30	Nanjing	0.41	0.38	0.52	1.36	1.45	1.35	0.52
31	Nanyang	0.51	0.39	0.45	1.06	1.39	1.21	0.55
32	Ningbo	0.37	0.38	0.73	1.41	1.35	1.46	0.56
33	Qingdao	0.35	0.39	0.44	1.36	1.47	0.75	0.51
34	Shanghai	0.41	0.46	0.32	1.38	1.15	1.34	0.56
35	Shenyang	0.43	0.46	0.53	1.25	1.42	1.61	0.58
36	Shenzhen	0.40	0.26	0.43	1.48	1.64	1.31	0.47
37	Shijiazhuang	0.46	0.50	0.56	1.13	1.37	1.25	0.54
38	Tianjin	0.46	0.46	0.44	1.30	1.38	1.16	0.57
39	Wuhan	0.47	0.44	0.31	1.29	1.30	1.54	0.54
40	Xi'an	0.29	0.31	0.36	1.61	1.67	1.65	0.46
41	Delhi	0.38	0.36	0.35	1.46	1.67	1.62	0.44
42	Kolkata	0.51	0.35	0.31	1.32	1.61	1.44	0.54
43	Jakarta	0.30	0.31	0.39	1.62	1.56	1.15	0.40
44	Tehran	0.30	0.60	0.59	1.70	1.27	1.46	0.55
45	Nagoya	0.41	0.35	0.37	1.53	1.53	1.43	0.46
46	Osaka	0.34	0.32	0.45	1.55	1.57	1.13	0.44
47	Tokyo	0.39	0.38	0.56	1.41	1.38	1.32	0.43
48	Seoul	0.24	0.47	0.26	1.72	1.47	1.62	0.52
49	Kuala Lumpur	0.41	0.29	0.32	1.48	1.66	1.68	0.46
50	Karachi	0.32	0.26	0.25	1.59	1.59	1.69	0.45
51	Lahore	0.40	0.25	0.38	1.53	1.72	1.46	0.48
52	Manila	0.28	0.35	0.29	1.69	1.58	1.33	0.46
53	Singapore	0.34	0.34	0.50	1.53	1.55	1.47	0.45
54	Bangkok	0.32	0.44	0.42	1.54	1.57	1.26	0.38
55	Istanbul	0.31	0.45	0.53	1.70	1.43	1.56	0.44
56	Hanoi	0.44	0.32	0.45	1.37	1.61	1.68	0.45
57	Ho Chi Minh City	0.49	0.32	0.26	1.40	1.66	1.55	0.49
58	Brisbane	0.36	0.45	0.45	1.39	1.56	1.39	0.43
59	Melbourne	0.38	0.44	0.38	1.55	1.54	1.67	0.45
60	Sydney	0.32	0.35	0.29	1.50	1.62	1.66	0.44
61	Vienna	0.34	0.32	0.32	1.51	1.67	1.54	0.45
62	Minsk	0.31	0.41	0.34	1.46	1.44	1.65	0.55
63	Brussels	0.39	0.37	0.39	1.47	1.61	1.54	0.46
64	Sofia	0.56	0.42	0.37	1.23	1.49	1.37	0.56
65	Zagreb	0.59	0.42	0.42	1.18	1.45	1.61	0.57
66	Prague	0.42	0.39	0.37	1.41	1.56	1.15	0.49
67	Paris	0.48	0.48	0.55	1.49	1.17	1.40	0.46
68	Berlin	0.42	0.41	0.40	1.48	1.49	1.52	0.51
69	Cologne	0.35	0.47	0.44	1.44	1.52	1.59	0.51
70	Hamburg	0.36	0.37	0.35	1.44	1.62	1.58	0.47
71	Munich	0.36	0.36	0.37	1.39	1.61	1.58	0.48
72	Athens	0.39	0.26	0.32	1.47	1.72	1.67	0.49
73	Budapest	0.46	0.28	0.31	1.36	1.67	1.61	0.51
74	Dublin	0.37	0.34	0.48	1.53	1.68	1.48	0.43
75	Milan	0.46	0.40	0.47	1.26	1.53	1.54	0.46
76	Rome	0.37	0.35	0.44	1.50	1.66	1.54	0.39
77	Amsterdam	0.41	0.33	0.26	1.38	1.60	1.67	0.46
78	The Hague	0.32	0.32	0.38	1.37	1.65	1.63	0.44
79	Oslo	0.38	0.38	0.27	1.56	1.59	1.70	0.51
80	Warsaw	0.41	0.28	0.28	1.45	1.61	1.68	0.48
81	Bucharest	0.42	0.33	0.34	1.44	1.65	1.63	0.51
82	Kazan	0.59	0.31	0.32	1.38	1.50	1.70	0.44
83	Moscow	0.25	0.40	0.41	1.70	1.51	1.38	0.44
84	Nizhniy Novgorod	0.59	0.41	0.39	1.20	1.43	1.48	0.52
85	Perm	0.57	0.34	0.36	1.14	1.62	1.50	0.55
86	Rostov	0.53	0.47	0.33	1.27	1.37	1.61	0.50
87	Saint Petersburg	0.30	0.51	0.47	1.68	1.39	1.40	0.54
88	Samara	0.63	0.58	0.49	1.07	1.26	1.38	0.66
89	Ufa	0.71	0.51	0.54	0.96	1.29	1.37	0.65
90	Volgograd	0.65	0.36	0.44	0.98	1.50	1.40	0.63
91	Voronezh	0.55	0.48	0.37	1.17	1.49	1.46	0.50
92	Belgrade	0.59	0.27	0.43	1.24	1.73	1.54	0.61
93	Barcelona	0.43	0.25	0.26	1.47	1.67	1.72	0.45
94	Madrid	0.32	0.37	0.30	1.61	1.48	1.67	0.42
95	Sevilla	0.52	0.38	0.34	1.27	1.46	1.51	0.48
96	Dnipro	0.59	0.43	0.31	1.10	1.54	1.63	0.56
97	Kyiv	0.43	0.29	0.38	1.36	1.62	1.60	0.48
98	Odesa	0.44	0.42	0.41	1.29	1.47	1.58	0.46
99	Birmingham	0.37	0.52	0.26	1.52	1.28	1.42	0.46
100	Birstall	0.64	0.40	0.45	1.01	1.60	1.46	0.66
101	Leeds	0.39	0.59	0.44	1.46	1.04	1.58	0.45
102	London	0.57	0.40	0.72	1.34	1.56	0.87	0.58
103	Manchester	0.34	0.38	0.40	1.52	1.57	1.49	0.46
104	Newcastle	0.39	0.25	0.41	1.45	1.66	1.56	0.52
105	Montreal	0.24	0.68	0.31	1.68	1.03	1.54	0.46
106	Toronto	0.50	0.51	0.47	1.36	1.43	1.24	0.61
107	Vancouver	0.42	0.26	0.59	1.37	1.69	1.29	0.57
108	Santo Domingo	0.41	0.50	0.27	1.49	1.36	1.72	0.50
109	Guatemala City	0.63	0.26	0.41	1.10	1.70	1.48	0.54
110	Guadalajara	0.37	0.71	0.50	1.36	1.04	1.68	0.48
111	Mexico City	0.34	0.26	0.28	1.47	1.65	0.93	0.66
112	Monterrey	0.34	0.30	0.74	1.62	1.64	1.63	0.54
113	Tijuana	0.43	0.34	0.26	1.49	1.61	1.59	0.48
114	Atlanta	0.47	0.27	0.30	1.44	1.68	1.31	0.44
115	Boston	0.27	0.73	0.39	1.37	0.97	1.56	0.44
116	Chicago	0.61	0.33	0.91	1.23	1.64	0.40	0.71
117	Dallas	0.30	0.46	0.73	1.60	1.45	1.46	0.44
118	Denver	0.36	0.45	0.37	1.44	1.19	1.25	0.58
119	Detroit	0.41	0.28	0.67	1.55	1.44	1.01	0.53
120	Houston	0.25	0.38	0.39	1.67	1.51	1.32	0.42
121	Los Angeles	0.37	0.53	0.42	1.60	1.58	1.51	0.56
122	Miami	0.31	0.66	0.68	1.52	1.43	1.10	0.55
123	Minneapolis	0.54	0.28	0.78	1.31	1.13	0.84	0.64
124	New York	0.34	0.30	0.36	1.68	1.64	1.50	0.43
125	Philadelphia	0.26	0.61	0.35	1.64	1.19	1.49	0.39
126	Phoenix	0.35	0.28	0.80	1.50	1.66	0.74	0.62
127	San Diego	0.45	0.24	0.35	1.44	1.76	1.57	0.45
128	San Francisco	0.30	0.64	0.24	1.61	1.16	1.66	0.46
129	Seattle	0.51	0.34	0.86	1.36	1.49	0.59	0.64
130	Tampa	0.43	0.37	0.50	1.35	1.58	1.20	0.49
131	Washington	0.26	0.40	0.31	1.60	1.55	1.48	0.40
132	Buenos Aires	0.40	0.46	0.49	1.62	1.54	1.39	0.49
133	La Paz	0.55	0.48	0.49	1.29	1.48	1.49	0.63
134	Santa Cruz	0.63	0.36	0.45	1.18	1.62	1.52	0.64
135	Belo Horizonte	0.49	0.41	0.30	1.39	1.53	1.69	0.55
136	Brasília	0.54	0.35	0.35	1.27	1.69	1.56	0.54
137	Fortaleza	0.31	0.31	0.45	1.57	1.62	1.52	0.42
138	Rio de Janeiro	0.47	0.36	0.26	1.47	1.51	1.68	0.44
139	Sao Paulo	0.33	0.31	0.41	1.65	1.57	1.37	0.41
140	Santiago	0.26	0.46	0.44	1.73	1.49	1.40	0.45
141	Bogota	0.52	0.61	0.48	1.41	1.25	1.39	0.63
142	Medellin	0.71	0.57	0.61	1.00	1.35	1.27	0.65
143	Quito	0.67	0.57	0.52	1.07	1.49	1.42	0.65
144	Lima	0.32	0.44	0.48	1.71	1.49	1.48	0.56

Supplementary Table 7. Pearson correlation matrix between road network pattern and socioeconomic & environmental indicators. *PropG − T* denotes proportion of gridiron, linear, chaotic, organic, radial, and tributary, respectively. *GDP*, *GDP per capita*, and *GNI per capita* are 2020 country data in current US dollar. *NTL* indicates the average nighttime light brightness in the study boundary. *Population* refers to the total population of cities. *Pop. growth* is the population growth rate within the 15 km city boundary from 2010 to 2020. *PM*2.5 denotes the annual average PM2.5 density (mostly in 2019). The values are the Pearson correlation coefficients (ρ), while the * behind indicates the p-value significance (*: significant, p<=0.05).

	Prop_G	Prop_L	Prop_C	Prop_O	Prop_R	Prop_T	PDP	PDI	GNSI
GDP	0.324 (*)	-0.073	-0.415 (*)	0.048	-0.009	0.169 (*)	0.049	-0.179 (*)	0.041
GDP per capita	0.449 (*)	-0.346 (*)	-0.422 (*)	-0.057	0.416 (*)	0.087	-0.046	0.069	-0.257 (*)
GNI per capita	0.458 (*)	-0.351 (*)	-0.424 (*)	-0.058	0.42 (*)	0.082	-0.043	0.064	-0.252 (*)
NTL	0.312 (*)	-0.482 (*)	-0.444 (*)	0.415 (*)	0.503 (*)	-0.248 (*)	-0.03	0.024	-0.217 (*)
Population	0.031	-0.305 (*)	-0.338 (*)	0.454 (*)	0.242 (*)	-0.06	-0.023	-0.087	-0.147
Pop. growth	0.145	0.017	0.202 (*)	-0.156	-0.215 (*)	-0.172 (*)	0.14	-0.189 (*)	0.196 (*)
PM2.5	-0.25 (*)	0.297 (*)	0.026	0.064	-0.359 (*)	0.152	-0.017	-0.078	0.157

Supplementary Table 8. Pearson correlation matrix between road network pattern and socioeconomic & environmental indicators (excluding the US cities).

	Prop_G	Prop_L	Prop_C	Prop_O	Prop_R	Prop_T	PDP	PDI	GNSI
GDP	-0.372 (*)	0.189 (*)	-0.331 (*)	0.239 (*)	-0.266 (*)	0.453 (*)	0.032	-0.252 (*)	0.117
GDP per capita	0.031	-0.247 (*)	-0.338 (*)	0.083	0.432 (*)	0.284 (*)	-0.118	0.146	-0.352 (*)
GNI per capita	0.03	-0.255 (*)	-0.342 (*)	0.087	0.443 (*)	0.286 (*)	-0.118	0.144	-0.351 (*)
NTL	0.144	-0.452 (*)	-0.393 (*)	0.528 (*)	0.529 (*)	-0.204 (*)	-0.112	0.097	-0.292 (*)
Population	0.161	-0.337 (*)	-0.383 (*)	0.438 (*)	0.259 (*)	-0.057	-0.006	-0.115	-0.163
Pop. growth	0.334 (*)	-0.01	0.188 (*)	-0.175	-0.22 (*)	-0.198 (*)	0.17	-0.217 (*)	0.217 (*)
PM2.5	-0.163	0.281 (*)	-0.01	0.004	0.358 (*)	0.124	-0.035	-0.072	0.157

Supplementary Table 9. Pearson correlation matrix between road network pattern and socioeconomic & environmental indicators (excluding Chinese cities).

	Prop_G	Prop_L	Prop_C	Prop_O	Prop_R	Prop_T	PDP	PDI	GNSI
GDP	0.622 (*)	-0.291 (*)	-0.384 (*)	-0.107	0.202 (*)	-0.067	0.043	-0.085	-0.047
GDP per capita	0.399 (*)	-0.341 (*)	-0.521 (*)	0.009	0.371 (*)	0.239 (*)	-0.041	0.015	-0.234 (*)
GNI per capita	0.409 (*)	-0.348 (*)	-0.524 (*)	0.008	0.375 (*)	0.233 (*)	-0.039	0.01	0.228 (*)
NTL	0.284 (*)	-0.464 (*)	-0.482 (*)	0.468 (*)	0.485 (*)	-0.25 (*)	-0.038	-0.007	-0.203 (*)
Population	0.109	-0.423 (*)	-0.318 (*)	0.469 (*)	0.334 (*)	-0.202 (*)	-0.05	-0.023	-0.191 (*)
Pop. growth	0.144	0.05	0.218 (*)	-0.182 (*)	-0.248 (*)	-0.191 (*)	0.145	-0.209 (*)	0.211 (*)
PM2.5	-0.081	0.134	0.17	-0.024	-0.171	-0.082	-0.075	0.103	0.03

References

1. Chen, W., Wu, A. N. & Biljecki, F. Classification of urban morphology with deep learning: Application on urban vitality. *Comput. Environ. Urban Syst.* **90**, 101706, DOI: 10.1016/j.compenvurbsys.2021.101706 (2021).

2. Cardillo, A., Scellato, S., Latora, V. & Porta, S. Structural properties of planar graphs of urban street patterns. *Phys. Rev. E* **73**, 066107 (2006).

3. Eppstein, D. & Goodrich, M. T. Studying (non-planar) road networks through an algorithmic lens. In *Proceedings of the 16th ACM SIGSPATIAL international conference on Advances in geographic information systems*, 1–10 (2008).

4. Wu, A. N. & Biljecki, F. Ganmapper: geographical data translation. *Int. J. Geogr. Inf. Sci.* (2022).

5. He, K., Zhang, X., Ren, S. & Sun, J. Deep residual learning for image recognition (2015). 1512.03385.

6. He, K., Zhang, X., Ren, S. & Sun, J. Identity mappings in deep residual networks (2016). 1603.05027.

7. Chen, Z. *et al.* An extended time-series (2000-2018) of global NPP-VIIRS-like nighttime light data, DOI: 10.7910/DVN/YGIVCD (2020).